Z_{DR} calibration issues in the WSR-88Ds

Report on 2013-MOU

Valery Melnikov, Dusan Zrnic, Mike Schmidt, and Richard Murnan

30 September, 2013

Contents

1. Introduction

The National Weather Service has finished upgrading the WSR-88D radars to dual polarization. The upgraded radars are capable of measuring three new parameters, i.e., differential reflectivity, the differential phase, and correlation coefficient in addition to reflectivity, the Doppler velocity, and spectrum width. The three new polarimetric variables enable hydrometeor classification, recognition of non-meteorological echoes, and more accurate estimation of precipitation.

Measured differential reflectivity, Z_{DR}, and the differential phase depend on radar hardware and need calibrations. Accuracy of Z_{DR} measurements of ±0.1 dB allows achieving measurement accuracy of the rate of light precipitation about 10-15%. For more intense precipitation, accuracy of Z_{DR} measurements can be relaxed to about $0.1Z_{DR}$ if $Z_{DR} > 1$ dB. The accuracy of 0.1 dB is also needed to distinguish between types of snow. Thus, ±0.1 dB is the desired accuracy of Z_{DR} measurements.

A polarimetric scheme with simultaneous transmission and reception of horizontally and vertically polarized waves, implemented on the WSR-88Ds, has two polarimetric channels consisting of similar but physically different devices that have to be calibrated. Three methods of Z_{DR} calibration are in use on different polarimetric weather radars: 1) calibration with built-in radar equipment, 2) observations of precipitation with a vertically looking radar antenna, and 3) use of cross-polarization measurements. The first method has been implemented on the WSR-88Ds by the manufacturer. The second approach cannot be used on the WSR-88D because the maximum elevation angle of its antenna is 60^o. The third method is under development.

The aim of this paper is to analyze the implemented Z_{DR} calibration method which is referred to as baseline calibration. The Radar Operations Center, ROC, monitors Z_{DR} system bias obtained with the baseline calibration. It shows that the mean Z_{DR} system bias across the network is close to zero suggesting there is no a major flaw in the baseline calibration. At the same time, a scatter in the system Z_{DR} biases is observed and some radars have unacceptably large system Z_{DR} biases. To reduce this scatter, understanding of its origin is needed. In this paper, the baseline Z_{DR} calibration is described (section 2) and analyzed (section 3). Weak links in the calibration procedures are identified and future work to eliminate possible uncertainties is outlined (section 3).

It is desirable to verify radar Z_{DR} calibration. One of the verifications available is radar observations of light precipitation. The method is based on a relation between reflectivity, Z, and Z_{DR}; briefly: Z of 20 dBZ should have Z_{DR} of 0.2 dB or less. This method is used by the ROC to verify the system Z_{DR} bias. The deficiency of this approach is that even light rain/drizzle can have a small number of large droplets that can bias Z_{DR} high. The scatter in the observed system Z_{DR} biases can be due to uncertainties in the Z - Z_{DR} relation for different types of precipitation. In this paper, two additional methods for verification of Z_{DR} calibration are considered: 1) radar observations of clear-air returns and 2) Z_{DR} measurements of the Moon (section 4).

2. System baseline Z_{DR} calibration

A simplified diagram of the measurement paths of the system Z_{DR} baseline calibration is shown in Fig. 1. There are two distinct electronic blocks involved in the measurements: antenna mounted electronics (AME) and RF pallet. Both devices are mounted on the antenna. AME contains built-in generators and amplifiers to be used as test signal sources in calibration (the left upper corner of Fig. 2.1), the Power Sense, and Receiver (they are shown with the dashed rectangles).

For accurate measurements of differential reflectivity of hydrometeors, it is necessary to correct for a bias introduced by signal differences in the transmit and receive paths. These differences will be called biases or offsets. Z_{DR} calibration procedure consists of a sequence of measurements for obtaining system biases. The sequence must be performed by trained technicians and consists of the following procedures.

- Measurements of AME test signal powers (R33 and R34 dBm)
- Power Sense calibration (R286, R287, R289 dB)
- RF pallet broadband loss (R288 dB)
- AME noise source ENR calibration (R35, R299 dB)
- Straight and cross measurements (R297, R298 dB)
- Solar flux measurement results (A031 dB)

Parameters Rxxx above are: equivalent signal gains or losses measured in dB, signal power levels measured in dBm, or Noise source ENR measured in dB. These parameters are measured throughout off-line calibrations and introduced into the radar adaptation table to be used as a fixed part of system Z_{DR} bias. In this section of the report, the above procedures are described per document NWS EHB 6-510 section 6.6 Calibration. All references on sections and measurement procedures correspond to that document. The calibration procedures begin with calibrating an external signal noise generator and a power meter described in section 6.6.3.3.3 (page 6-340); these procedures are basic engineering operations and are not discussed herein.

Z_{DR} calibration consists of calibrating 1) the paths from the transmitter to the couplers above the circulators; that bias is denoted as TXB (transmit bias), 2) the paths from the couplers to the input to RVP8, RCB (receive bias), and 3) the two way path between the couplers and outside of the radome denoted with SMB (Sun measurement bias). Sun measurements are needed to complete the calibration. Z_{DR} of the Sun is 0 dB and therefore unbiased measurements of the antenna/feed can be made. The measurements of TXB, RCB, and SMB are relative, t.e., the difference of channel signals is measured, not the absolute signals. The main equation for the system Z_{DR} bias is written as (section 5.5.3.6.12)

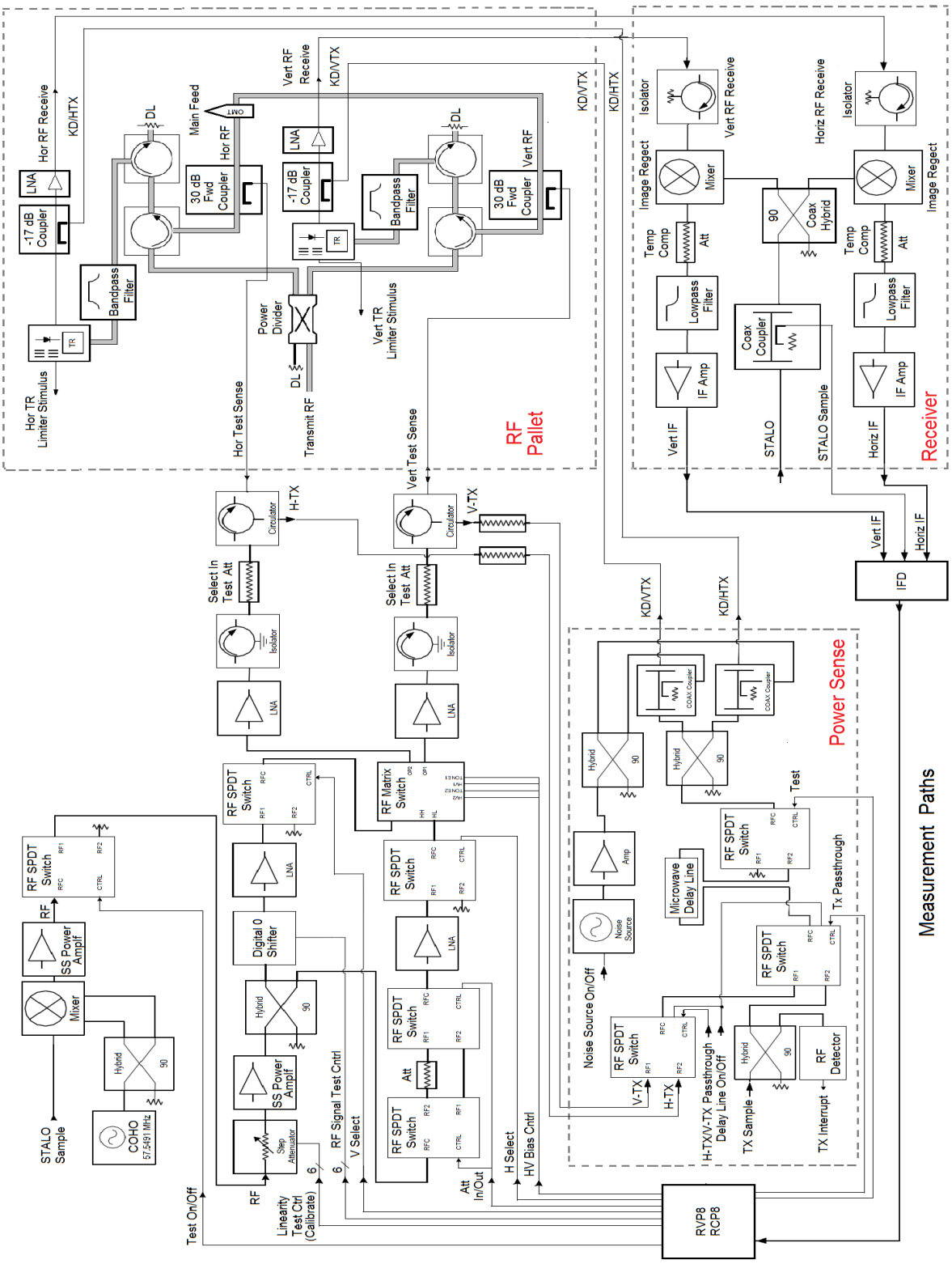

Fig. 2.1. Measurement paths in system Z_{DR} calibration, simplified diagram.

$$Z_{DR\text{-}SYS} = 2\,SMB + RCB + TXB. \quad (1)$$

SMB enters with coefficient 2 because the sun measurement bias accounts for the system part that is in both transmit and receive paths. This system part includes the waveguides above the 30-dB couplers in the RF Pallet, feed-horn, antenna, and radome. Measurements to obtain three addends in (1) are described below per the document. This document does not contain justifications for the measurements; possible explanations of the calibrations are provided in this report.

The critical system part in the Z_{DR} calibration is the RF Pallet which is the central block in the diagrams in Fig. 2.2. To aid in considerations of the procedures, signal paths in all calibration procedures are shown in the diagrams with a thick blue line. Some notations are introduced in this report to justify the measurements and are also used in the analysis of the measurements and recommendations provided in section 3 of this report.

2.1. Measurements of AME test signal powers (R33 and R34)

In this procedure of the off-line calibration (6.6.3.3.7, page 6-347), the powers R33 and R34 that are supplied to the RF Pallet from AME are calibrated/measured. R33 is the calibrated power injected into the Vertical polarization channel and R34 is the calibrated power injected into the Horizontal channel. The signal source is the AME RF CW built-in generator. The measurement device is an external RF power meter.

To measure R34, cable 2W575 is disconnected from the 30-dB coupler and connected to a power meter (Fig. 2.2). To measure R33, cable 2W574 is disconnected from the 30-dB coupler and connected to a power meter (Fig. 2.2, the signal path is shown with the thick blue line). Powers R33 and R34 must be long time stable since these powers are injected to RF pallet every 5-6 minutes in between the VCPs to calibrate the receive paths of the system. The RF CW source is placed into a climate control box of AME. R34 is used to determine the receiver gain for Reflectivity calculation (based upon horizontal returns). R33 and R34 are also used for system health checks. R33 and R34 are not used for ZDR, differential phase or correlation coefficient.

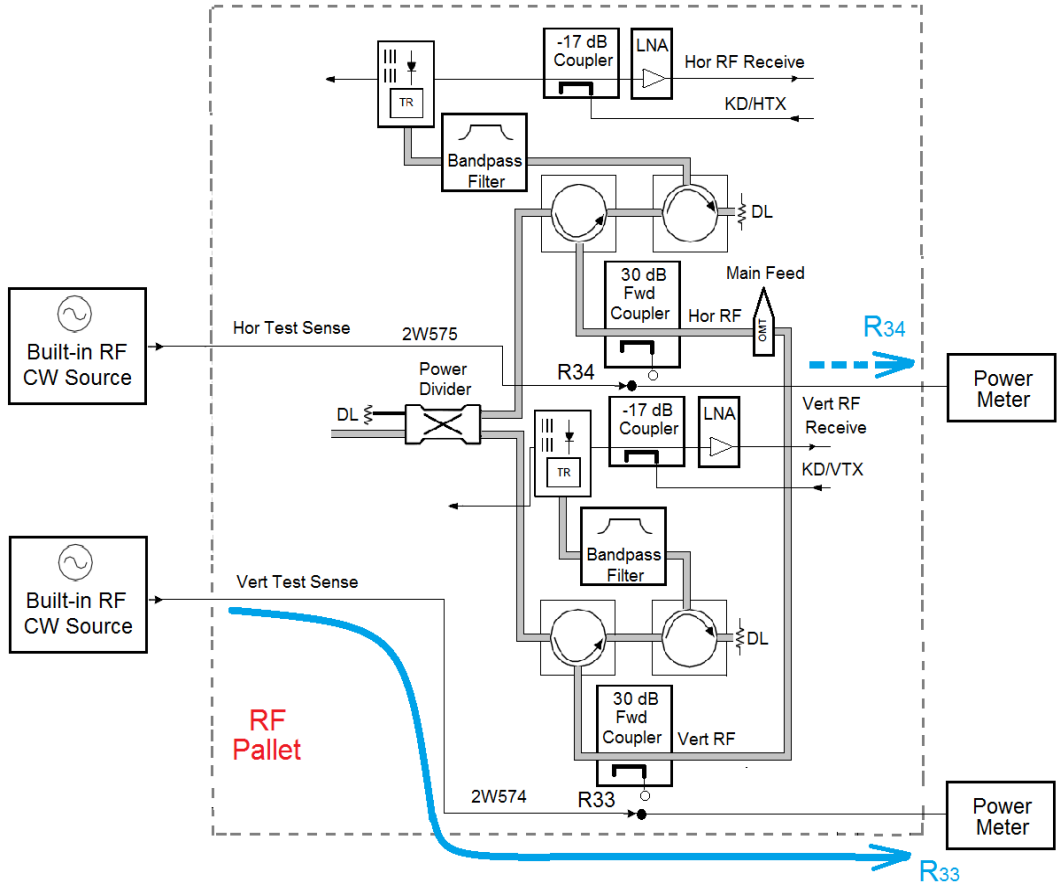

Fig. 2.2. Measurements of AME test signal powers (R33 and R34).

2.2. Power Sense calibration (R286, R287, and R289)

These off-line measurements (6.6.3.3.8, page 6-355) calibrate the losses in the Horizontal and Vertical transmitter pulse peak power channels including RF Pallet, Power Sense, and Receiver. The signal source is the system klystron. The procedure consists of two parts. In part 1, the measurement device is an external RF power meter connected to the coupled port of the 30-dB coupler (Fig. 2.3). In part 2, the power on the same coupled port of the 30-dB coupler is measured via BITE circuitry with signal processor RVP8. These measurements do not include a part of the system above the 30-dB coupler, i.e., the feed-horn, antenna, radome, and corresponding waveguides. These devices are calibrated via solar measurements (see section 2.6).

Part 1, Consider measurements in the vertical radar channel; similar operations are conducted in the horizontal channel (Fig. 2.3). The power in the vertical channel (P_{287}) is measured at the coupled port of the 30-dB coupler. The signal path is shown in Fig. 2.3 with the thick blue line. Cable 2W574 is disconnected from the 30-dB coupler and a calibrated power meter is connected

to the coupler. The transmitter is turned on and power P_{287} (denoted in the document as Vertical TX power) is measured with an average power meter. An additional 20-dB attenuator must be connected to protect the power meter's input since the peak power level at the 30-dB coupler is on the order of +53dBm. Actual loss of the 20-dB attenuator is measured using an external RF generator; this is done before making the Power Sense measurements. The peak power in the channel, denoted in the document as V Peak, is obtained as (page 6-367),

$$\text{V Peak} = P_{287} - 20\ \text{dB} - \text{DutyCycle}, \qquad (2)$$

where P_{287} is the power meter reading, 20 dB is the attenuator loss (actual measured value must be used), and DutyCycle is the duty cycle of transmitter that is obtained from a window on the technician laptop. (DutyCycle is a byproduct of transmitter pulse alignment measurements and procedures not covered in this document). Simultaneously with V Peak, the burst pulse power Pbv_1 is obtained as a number in the laptop window.

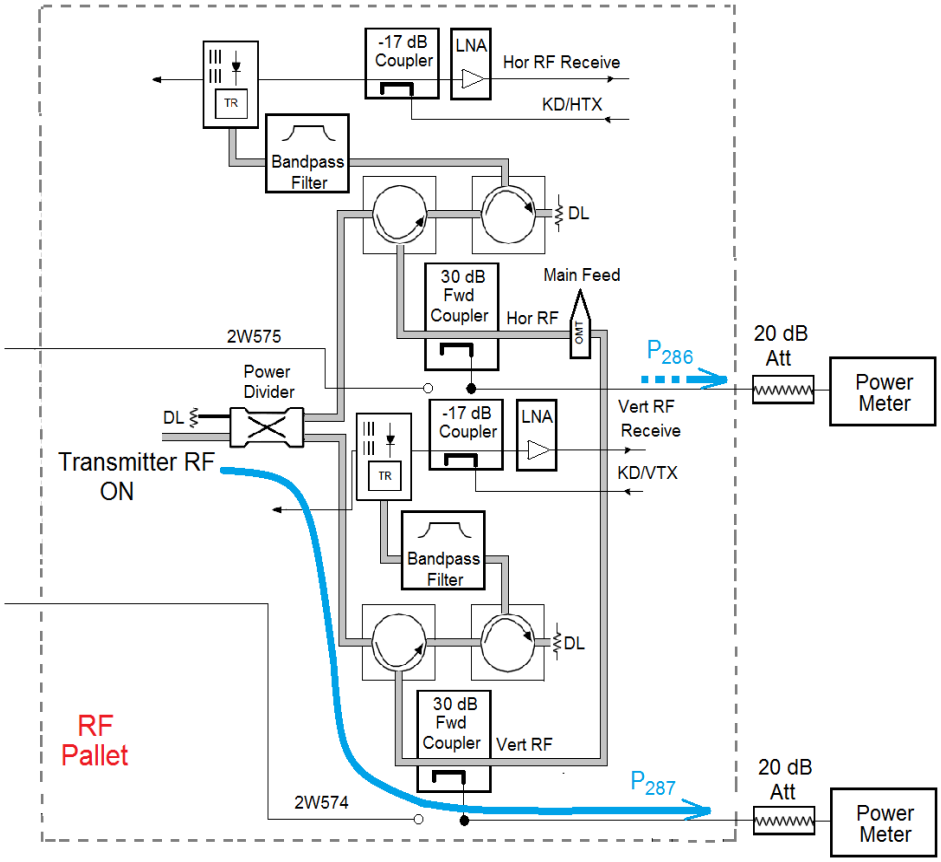

Fig. 2.3. Part 1 of the Power Sense calibration.

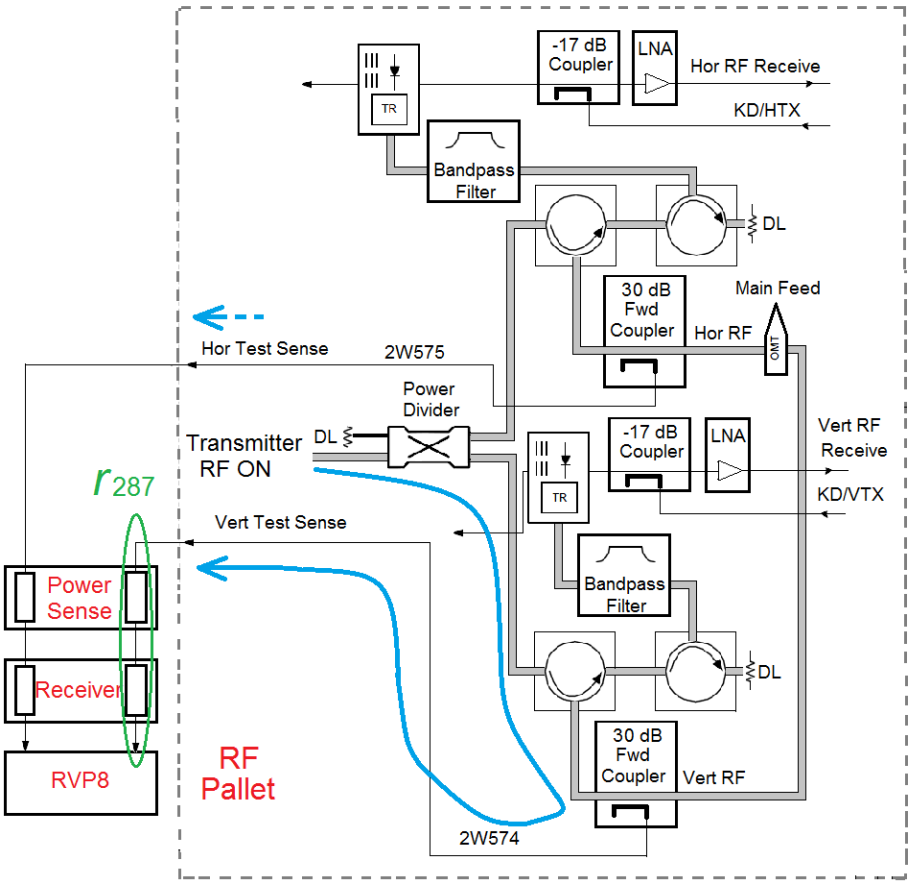

Fig. 2.4. Part 2 of the Power Sense calibration.

Part 2. The external power meter is disconnected from the 30-dB coupler, and cable 2W574 is reconnected to the 30-dB coupler (Fig. 2.4). The power from the 30-dB coupler is again measured using the BITE path which measures the peak power with the RVP8. The power in the vertical channel Pv (denoted in the docs as Vertical Power) is measured with the signal processor and is shown in the laptop window. In the window, corresponding burst pulse Pbv_2 is shown also and used to normalize any transmitter output power differences between Part 1 and Part 2 (i.e. measurement bias is possible if the transmitter isn't fully warmed up). Vertical Power Sense Offset R287 is obtained as,

$$R287 = Pv - Pbv_2 + Pbv_1 - V\ Peak. \quad (3)$$

The same measurements are made for the horizontal channel and R286 is obtained from the following

$$H\ Peak = P_{286} - 20\ dB - DutyCycle, \quad (4)$$

$$R286 = Ph - Pbh_2 + Pbh_1 - H\ Peak. \quad (5)$$

Powers Ph and Pv are measured with RVP8 and read in from the laptop window. R289 is the Horizontal power measured with the RVP8:

$$R289 = Ph. \quad (6)$$

Rationale. There is no justification for these measurements in the document. A possible explanation follows. Let Pt_1 be the total transmitter power at its output during **Part 1** of the measurements. Replicas of the transmitter RF pulses are taken as the burst pulses and supplied to two radar channels. The Tx pulse burst power is sampled pre-RF Pallet division and is measured by the IFD as a peak power measurement. The horizontal and vertical burst power use the exact same measurement path and is measured by the same IFD input. The only difference is that vertical burst is sampled at the same time as vertical power sense. Similarly, horizontal burst is sampled at the same time as horizontal power sense. Power Sense is programmed to sample: 1. Horizontal power (and burst) 2. Vertical power (and burst) 3. RF Pallet input power. H and V burst will be the same if the transmitter output power is the same during the horizontal and vertical parts of this off-line calibration. However, it is possible (and likely on older klystrons) that the klystron is in a warm-up state during the physical measurements causing different power levels measurements during the different stages of this calibration. The burst powers are used to normalize the measurements. If the transmitter power is exactly the same throughout the different stages of this calibration then the burst powers drop out of the equation. If, however, the transmitter power changes between stage 1 and stage 2, then the burst power calculation will compensate for the difference).

For the vertical channel, Pbv_1 can be represented as

$$Pbv_1 = Pt_1 + Abv \quad (7)$$

where Abv is the attenuation losses (a negative number) for the burst pulse in the channel.

Radar pulse Pt_1 comes to the power divider in RF Pallet through long waveguides and the rotary joints; all these losses denote as Lw (a negative number). So the power Ptd_1 at the divider's input is

$$Ptd_1 = Pt_1 + Lw. \quad (8)$$

The divider splits the power and a part Pdv_1 of it comes out from the divider:

$$Pdv_1 = Ptd_1 + Dv, \quad (9)$$

where Dv is the loss due to the power split. This power is attenuated by the waveguides, circulator, and 30-dB coupler with the total loss L_{287}. The power meter measures the mean power P_{287} that can be represented as,

$$P_{287} - \text{DutyCycle} + 20\ \text{dB} = Pdv_1 + L_{287}. \quad (10)$$

DutyCycle is the duty cycle of the transmitter in dB. For instance, for the short radar pulse (τ = 1.54 us) and pulse repetition frequency of 1000 Hz (PRT = 1 ms), the duty cycle is 1.54×10^{-3} = -28.12 dB. The duty cycle is needed to recalculate the mean measured power P_{287} to the peak pulse power V Peak which is measured at the coupled port of 30-dB coupler (this is not the peak power in the waveguide)

$$V\ Peak = P_{287} - \text{DutyCycle} + 20 \quad (11)$$

One can see that the latter differs from (2) by the sign at 20 and is a typo in (2) which does not affect the final result as it will be shown later. This 20 can considered as the loss of 20-dB attenuator (a negative number); then the sign is plus as in the document. Using eqs. (7) to (10), V Peak can be represented as

$$V\ Peak = Pbv_1 + Abv + Lw + Dv + L_{287}. \quad (12)$$

Now consider **Part 2** of the measurements with the transmitter power Pt_2 that can deviate from Pt_1. This deviation can be obtained from difference between the powers of burst pulses Pbv_1 and Pbv_2. The peak power at the coupled port of 30-dB coupler can be represented similarly to (12)

$$V\ Peak_2 = Pbv_2 + Abv + Lw + Dv + L_{287}. \quad (13)$$

This power comes to RVP8 trough the Power Sense and Receiver with sum amplification of r_{287} so that the measured power Pv is

$$Pv = V\ Peak_2 + r_{287.} \quad (14)$$

One can obtain of r_{287} from (13) and (14):

$$r_{287} = Pv - Pbv_2 - (Abv + Lw + Dv + L_{287}). \quad (15)$$

Losses $Abv + Lw + Dv + L_{287}$ can be obtained from (12) and (11) from Part 1 of the measurements. Finally,

$$r_{287} = Pv - Pbv_2 + Pbv_1 - V\ Peak. \quad (16a)$$

For the horizontal channel,

$$r_{286} = Ph - Pbh_2 + Pbh_1 - H\ Peak. \quad (16b)$$

One can see that (16) coincides with (3) and (5), so r_{287} is indeed R287 and r_{286} is R286 in the document. The only difference is in +20 dB in (11) whereas it is -20 in (2). This difference does not play a role because the difference R287 - R286 is used. R286 is used for reflectivity

calibration (horizontal returns only with +/- 1 dB accuracy spec). R287 and R286 are also used for health checks and alarms.

2.3. RF Pallet broadband loss (R288)

This (6.6.3.3.9, page 6-368) measures losses in the circulators, bandpass filter, and receiver limiter in RF Pallet. The signal path is shown in Fig. 2.5 with the thick blue line. The signal source is the built-in RF CW generator and the measurement device is external power meter connected to the limiter through a 10-dB attenuator. It is not clear why these measurements are called “broad band loss” because a CW generator is used.

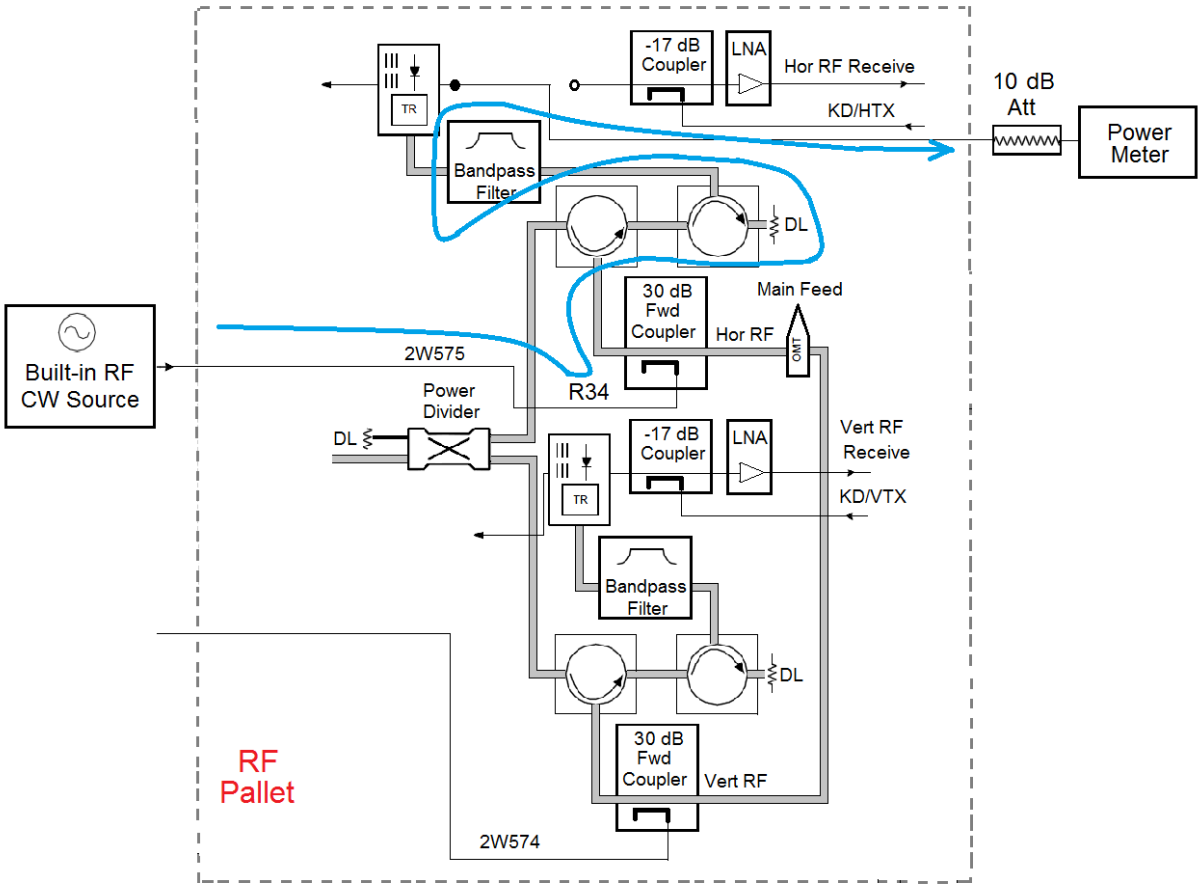

Fig. 2.5. Diagram for RF Pallet broadband loss measurements.

To make these measurements, the Horizontal receiver limiter is disconnected from the input to LNA and an external power meter is connected to the output of the limiter. Signal power R34 at the coupled port of 30-dB coupler has already been measured (section 2.1 above) and the loss of

30-dB coupler R293 is known from calibrations in the factory. Actual loss of the external 10-dB attenuator A_{10} is measured during calibration of the power meter. The broadband loss R288 is calculated as

$$R288 = P_{288} - R34 - R293 - A_{10}, \quad (17)$$

where P_{288} is the power meter reading. R288 is measured for the horizontal channel only.

Rationale. Signal of power R34 is supplied to the coupled port of 30-dB coupler with loss R293. The power at the input to the power meter is

$$P_{288} = P34 + R293 + R288 + A_{10} \quad (18)$$

from which (17) follows.

2.4. AME Noise Source Calibration (R35, R299)

The Exess Noise Ratio (ENR) in the horizontal and vertical channels is measured with this procedure. The signal source is a calibrated external noise generator. The measurement device is processor RVP8.

These measurements consist of two parts. A diagram for **Part 1** is shown in Fig. 2.6 where the signal path is shown with the thick blue line. To make these measurements, the horizontal LNA is disconnected from the limiter and an external noise source is connected to the LNA's input. The external noise source is turned ON and noise power (H Nose Level) is measured with RVP8 and shown in the laptop window. The same procedure is conducted in the vertical channel and V Nose Level is measured.

To make **Part 2** of the measurements, the LNA is reconnected to the limiter. RF Pallet is not involved in the measurements. The built-in noise source in the Power Sense is turned on and Horizontal Noise ON is measured with RVP8 and obtained from the laptop window. The diagram of the measurements is shown in Fig. 2.7. AME Noise Source Horizontal ENR, R35, is obtained as,

$$R35 = \text{Horizontal Noise ON} + \text{Noise\_STD\_ENR} - \text{H Noise Level}, \quad (19)$$

where Noise_STD_ENR is obtained from calibration of the external noise generator (section 6.6.3.3.3.3). AME Noise Source Vertical ENR, R299, is obtained as,

$$R299 = \text{Vertical Noise ON} + \text{Noise\_STD\_ENR} - \text{V Noise Level}, \quad (20)$$

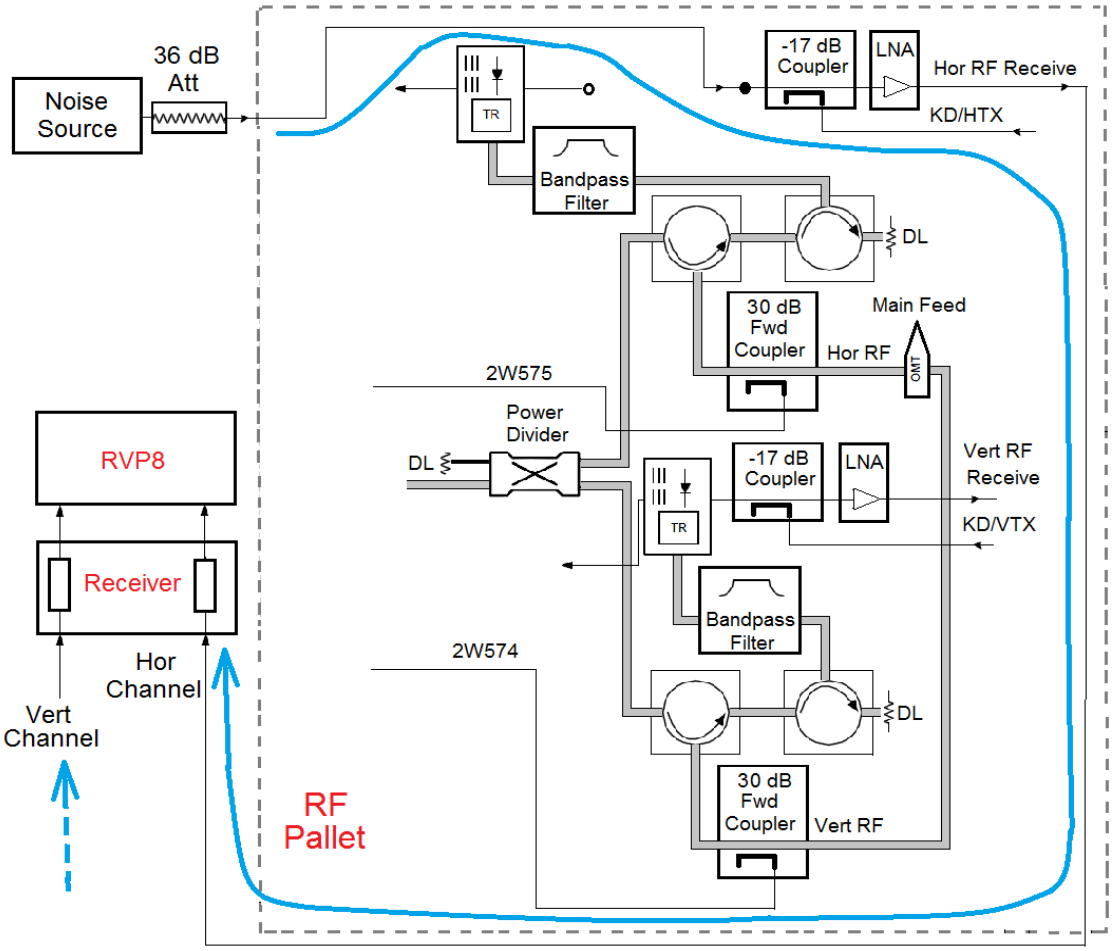

Fig. 2.6. Diagram for Part 1 of AME Noise Source calibration.

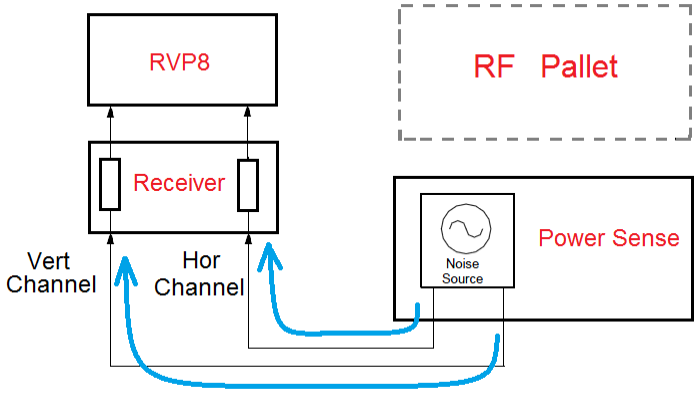

Fig. 2.7. Diagram for Part 2 of AME Noise Source calibration.

2.5. Cross and straight configuration measurements (R297, R298)

These measurements (6.6.3.3.11, page 6-382) calibrate the difference in the channel gains in receive (R297 – AME Test Signal Bias) and the difference in Power Sense gains in the channels (R298- Power Sense Calibration Offset Bias). R297 represents the difference H - V CW Test signal power as measured by the IFD. In concept, R297 should be the same as: R34 – R33. But R33 and R34 are measured with the average power meter which does not provide accurate enough or repeatable enough results necessary for Zdr accuracy. Using the results of crossed and straight, the H-V CW test signal power difference is measured on both the H receive channel and the V receive channel.

R298 represents a measurement path loss difference between the H Tx power measurement path and the V Tx power measurement path. Power Sense is programmed to record Tx pulse power measurements using the H receive path only so almost all of the Power Sense measurement path is common (i.e. from the output of the clutter module matrix switch -> delay line -> H LNA input coupler -> H Rx path -> H IFD power). R298 is the path difference for the non-common paths: [2W475 cable loss -> AME H Circulator -> AME H 30-dB attenuator -> H Power Sense matrix switch] - [2W474 cable loss -> AME V Circulator -> V 30-dB attenuator -> H Power Sense matrix switch].

Two signal sources are in use: built-in CW RF generator and the system transmitter. The measurement device is RVP8. These measurements are called "Cross-and-Straight' because cables 2W575 and 2W574 are connected to RF Pallet in cross (Fig. 2.8) and then straight (Fig. 2.10) configurations.

The measurements consist of four parts. **Part 1** is cross configuration measurements (Fig. 2.8) with cross connection of cables 2W575 and 2W574. The signal source is the built-in RF CW generator. The signal path for the measurements in the vertical channels is shown in Fig. 2.8 with the thick blue line. The measurement device is RVP8. The powers measured in the channels are H Power (measurable 9c in the document) denoted here as Pch_1 (power in the cross configuration in the horizontal channel in Part 1) and V Power (measurable 9d in the document) denoted herein as Pcv_1 (power in the cross configuration in the vertical channel in Part 1)

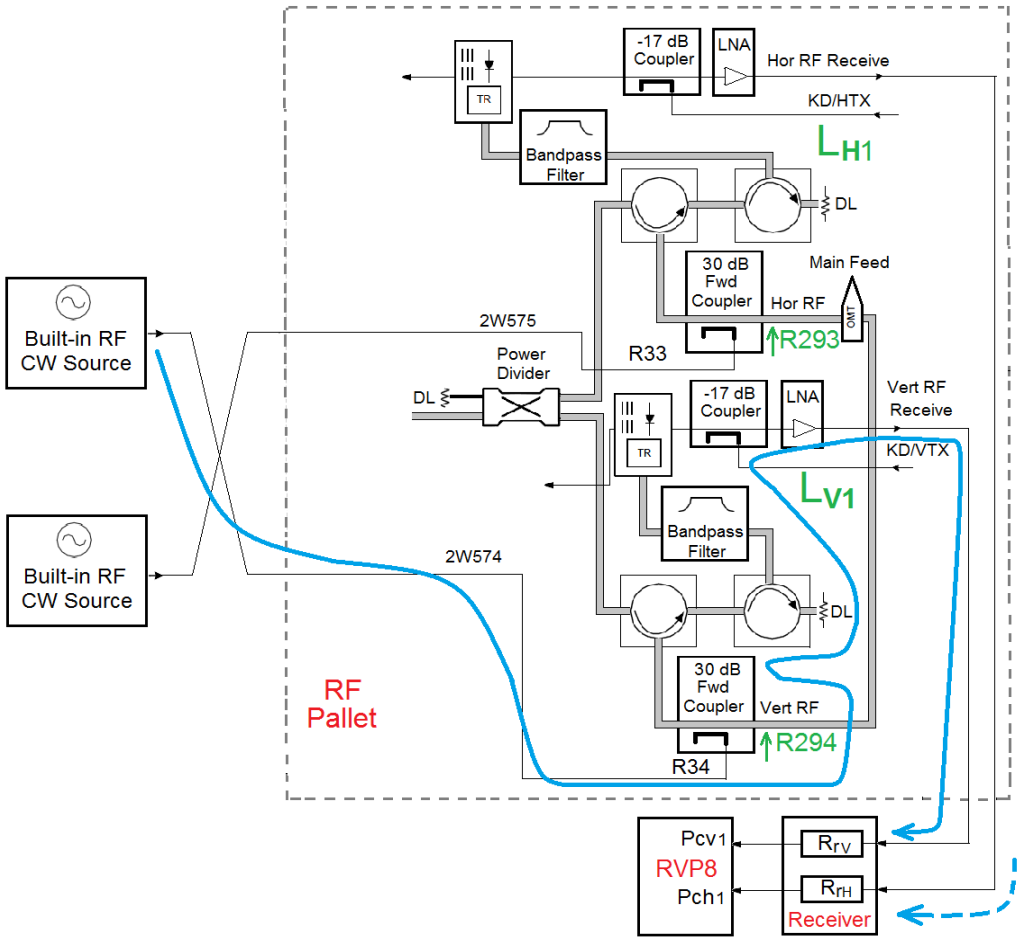

Fig. 2.8. Diagram for Part 1 of Cross-and-Straight calibrations.

Part 2 of the measurements (Fig. 2.9) is performed in the cross configuration but the signal source is the system klystron. The signal path is shown with the thick blue line. Two powers are measured with RVP8: Horizontal Power (measurable 9a in the docs) denoted here as Pch_2 (power in the cross configuration in the horizontal channel in Part 2) and Vertical Power (measurable 9b in the docs) denoted here as Pcv_2 (power in the cross configuration in the vertical channel in Part 2).

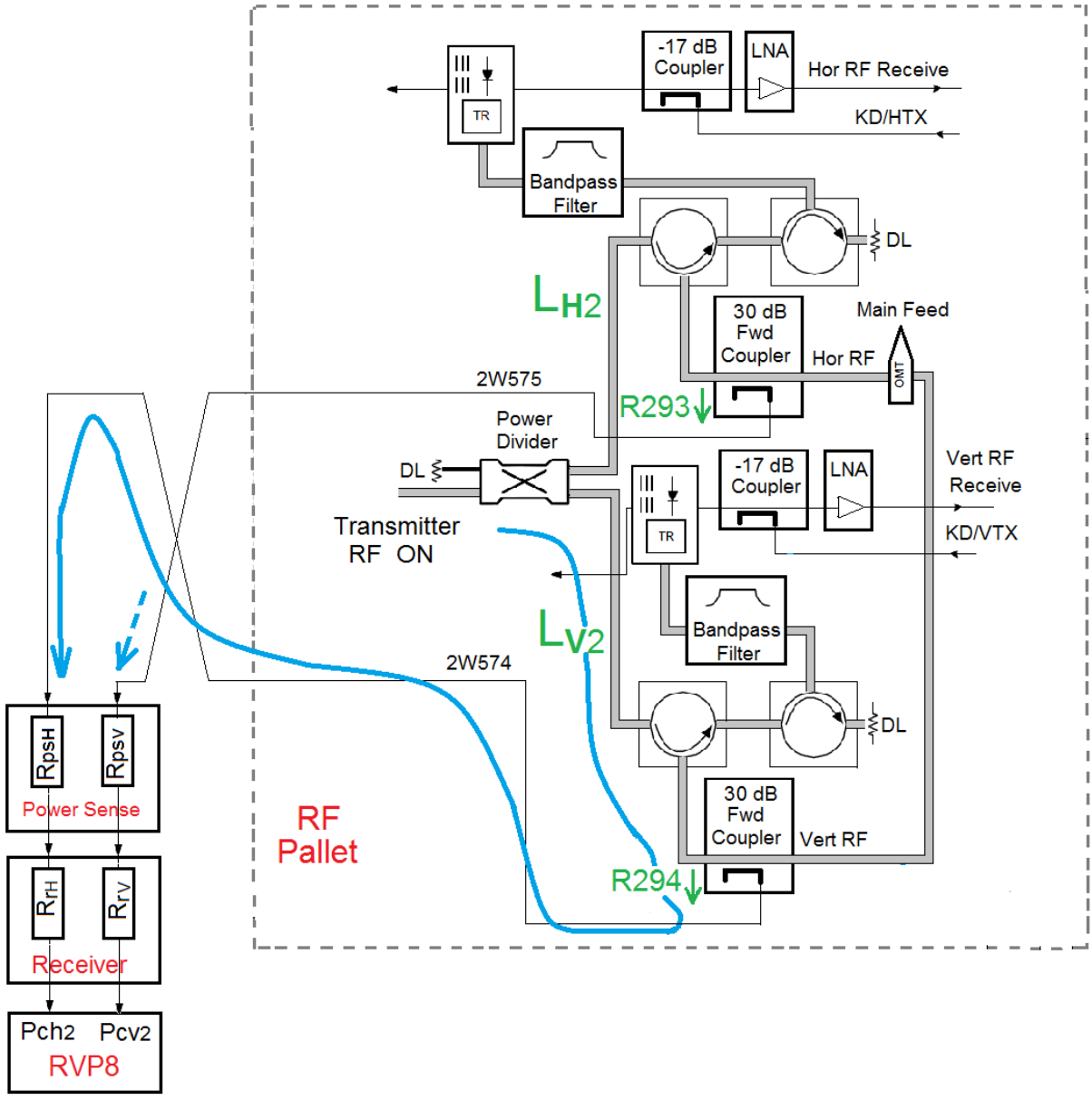

Fig. 2.9. Diagram for Part 2 of Cross-and-Straight calibrations.

Part 3 is performed in straight configuration of cables 2W575 and 2W574 (Fig. 2.10). The signal source is the built-in RF CW generator. The powers measured in the channels are H Power (measurable 10c in the document) denoted here as Psh_3 (power in the straight configuration in the horizontal channel in Part 3) and V Power (measurable 10d in the document) denoted herein as Psv_3 (power in the straight configuration in the vertical channel in Part 3).

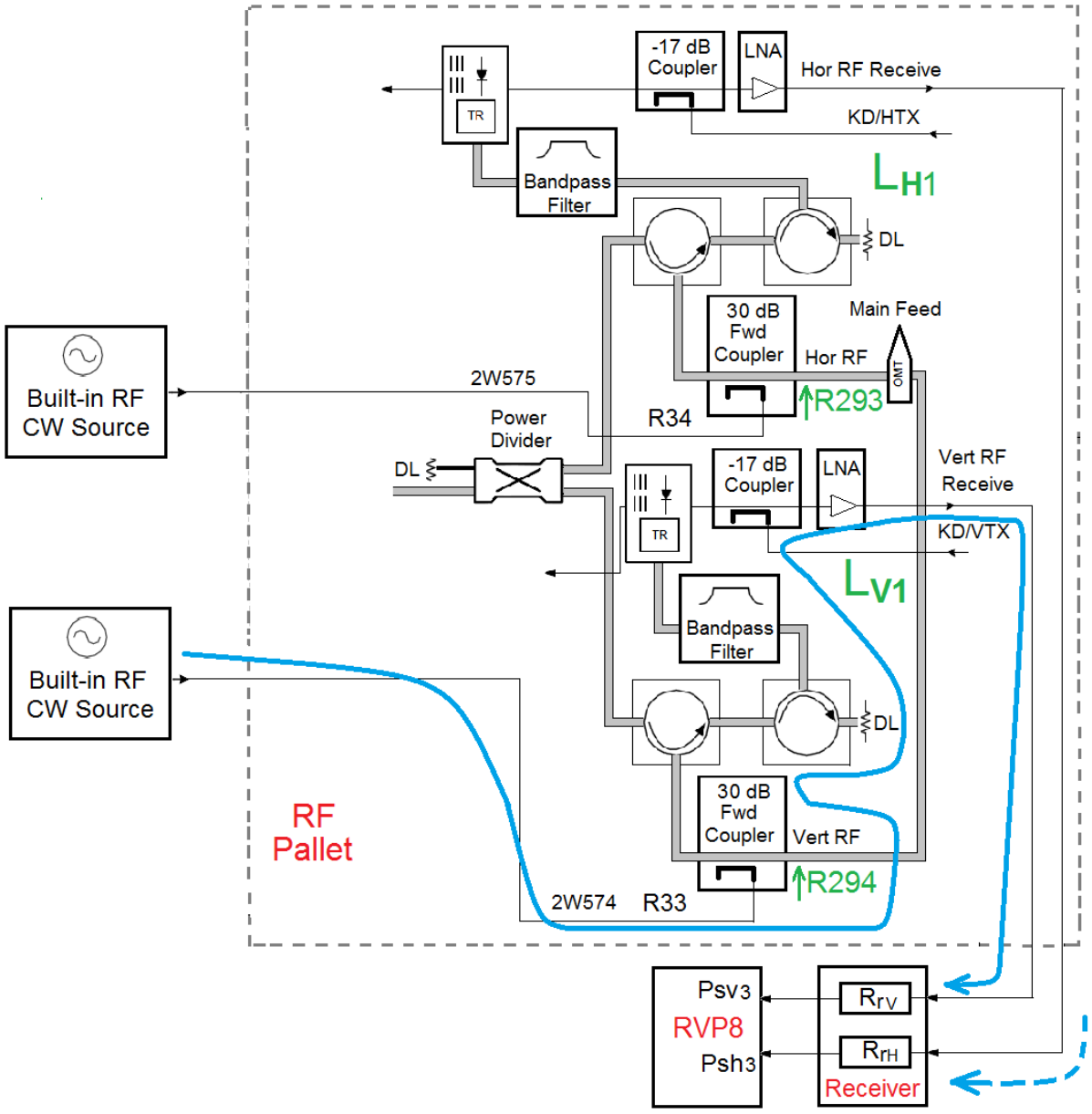

Fig. 2.10. Diagram for Part 3 of Cross-and-Straight calibrations.

Part 4 of the measurements (Fig. 2.11) is performed in the straight configuration but the signal source is the system klystron. Two powers are measured with RVP8: Horizontal Power (measurable 10a in the docs) denoted here as Psh_4 (power in the stright configuration in the horizontal channel in Part 4) and Vertical Power (measurable 10b in the docs) denoted here as Psv_4 (power in the straight configuration in the vertical channel in Part 4).

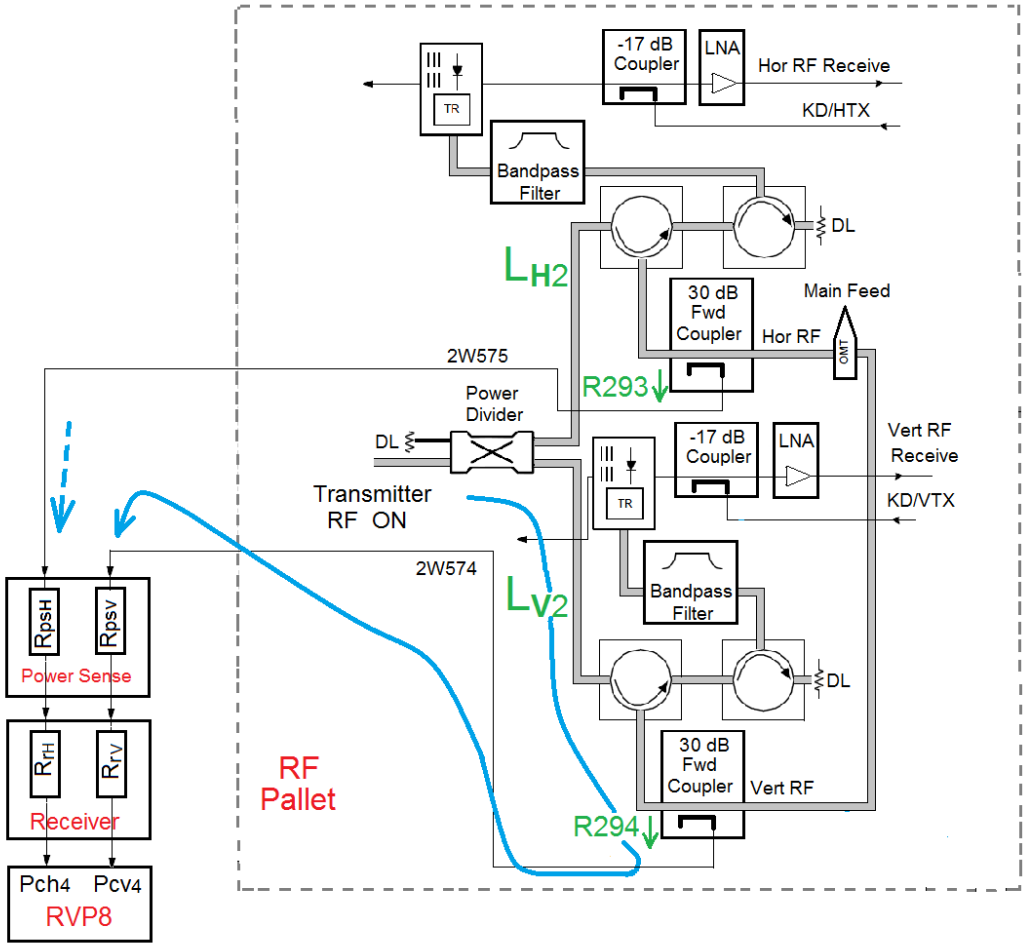

Fig. 2.11. Diagram for Part 4 of Cross-and-Straight calibrations.

These eight measured powers are presented in Table 1 with corresponding notations for further analysis.

Table 1. Notations of the measured powers in this report and corresponding short notations.

Measurement Part	Notation in the docs		Short notation herein
1	H Power	(meas. 9c)	P_{ch1}
	V Power	(meas. 9d)	P_{cv1}
2	H Power	(meas. 9a)	P_{ch2}
	V Power	(meas. 9b)	P_{cv2}
3	H Power	(meas. 10c)	P_{sh3}
	V Power	(meas. 10d)	P_{sv3}
4	H Power	(meas. 10a)	P_{sh4}
	V Power	(meas. 10b)	P_{sv4}

The following quantities are calculated from these 8 powers.

H-V Receiver bias (calc. 11a) = (meas. 10c) – (meas. 9c) = $P_{sh3} - P_{ch1}$, (21)

V-H Receiver bias (calc. 11b) = (meas. 9d) – (meas. 10d) = $P_{cv1} - P_{sv3}$, (22)

Signal Consistency Check (calc. 11c) = |(calc. 11a) – (calc. 11b)|, (23)

R297 = [(calc. 11a) + (calc. 11b)]/2, (24)

H-V Power Sense Bias (calc.12a) = (meas. 10a) – (meas. 9b) = $P_{sh4} - P_{cv2}$, (25)

V-H Power Sense Bias (calc.12b) = (meas. 9a) – (meas. 10b) = $P_{ch2} - P_{sv4}$, (26)

Power Sense Consistency Check (calc. 12c) = |(calc. 12a) – (calc. 12b)|, (27)

R298 = [(calc. 12a) + (calc. 12b)]/2, (28)

Calibration Consistency Check (calc. 13) = (calc. 11c) + (calc. 12c), (29)

The calibration Consistency check must be from 0.00 to 0.10 dB.

Rationale. Section 6.6 of the document does not provide justifications for these measurements. The following is a possible explanation. The goal of these measurements is obtaining the gains in the Receiver and Power Sense in each channel. This is needed because signal from weather comes to RVP8 through the RF Pallet and Receiver whereas test signals, that are used to calibrate the system in transmit, come to RVP8 through the Power Sense and Receiver.

Begin with **Part 1** of the measurements and recall that the built-in RF CW generator supplies powers R33 and R34 to the coupled port of 30-dB couplers in the straight configuration. Consider the signal path in vertical channel shown in Fig. 2.8 with the thick blue line. Power R34 is supplied to the input of 30-dB coupler in the vertical channel (in the straight configuration it is R33). Let L_{v1} be losses from the output port of the 30-dB coupler to the input of the receiver in the vertical channel. R293 and R294 (factory measured) are the losses of the 30-dB coupler in the channels (Fig. 2.8). Denote Rrv amplification in the receiver channel. Then the power P_{cv1} measured with RVP8 is

$$P_{cv1} = R34 + R294 + L_{v1} + Rrv. \quad (30)$$

Signal R33 is supplied to the input of the 30-dB coupler in the horizontal channel. Then P_{ch1} measured with RVP8 is

$$P_{ch1} = R33 + R293 + L_{h1} + Rrh, \quad (31)$$

Where Rrh is Receiver amplification in the channel and L_{h1} are the losses in all elements from the output from 30-dB coupler to the input of Receiver.

Consider now **Part 2** of the measurements (Fig. 2.9). Let Pv be the power at the output from the power divider in the vertical channel, $Lv2$ are the losses from the divider's output to the input of 30-dB coupler, and Rpsh is amplification in the Power Sense. Then the measured by RVP8 power is

$$Pch2 = Pv + Lv2 + R294 + Rpsh + Rrh. \quad (32)$$

By analogy with the latter and with obvious notations we can write for the power in the vertical channel of RVP8

$$Pcv2 = Ph + Lh2 + R293 + Rpsv + Rrv. \quad (33)$$

In **Part 3** of the measurements, cables 2W575 and 2W574 are reconnected in the straight configuration (Fig. 2.10). Power R33 is supplied to the coupled port of 30-dB coupler in the vertical channel. So the power $Psv3$ measured with RVP8 in the vertical channel is

$$Psv3 = R33 + R294 + Lv1 + Rrv. \quad (34)$$

In the horizontal channel, the measured power is

$$Psh3 = R34 + R293 + Lh1 + Rr_H. \quad (35)$$

Now write down the measured powers in **Part 4** of the measurements. By analogy with (32) and (33), the measured powers are

$$Psh4 = Ph + Lh2 + R293 + Rpsh + Rr_H. \quad (36)$$

$$Psv4 = Pv + Lv2 + R294 + Rpsv + Rrv. \quad (37)$$

We have 8 measured powers (30)-(37). By subtracting (30) from (31) and also subtracting (34) from (35) we obtain

$$Pch1 - Pcv1 = R33 - R34 + (Lh1 + R293 + Rr_H) - (Lv1 + R294 + Rrv), \quad (38)$$

$$Psh3 - Psv3 = R34 - R33 + (Lh1 + R293 + Rr_H) - (Lv1 + R294 + Rrv). \quad (39)$$

$Lh1 + R293 + Rr_H$ and $Lv1 + R294 + Rrv$ are the gains in the horizontal and vertical channels including the 30-dB couplers. The difference between the powers of calibrated signals is denoted as R297, i.e.,

$$R297 = R33 - R34. \quad (40)$$

Subtracting (39) from (38) one gets

$$R297 = (Psh3 - Psv3 - Pch1 + Pcv1)/2. \quad (41)$$

It is also seen that the difference in channel gains including the 30-dB couplers is

$$(Lh_1 + R293 + Rr_H) - (Lv_1 + R294 + Rrv) = (Pch_1 - Pcv_1 + Psh_3 - Psv_3)/2. \quad (42)$$

Subtracting Psv_4 from Pch_2 and Pcv_2 from Psh_4 one gets

$$Pch_2 - Psv_4 = (Rpsh + Rr_H) - (Rpsv + Rrv), \quad (43)$$

$$Psh_4 - Pcv_2 = (Rpsh + Rr_H) - (Rpsv + Rrv), \quad (44)$$

from which ir298 is obtained

$$r298 = (Rpsh + Rr_H) - (Rpsv + Rrv) = (Pch_2 - Psv_4 + Psh_4 - Pcv_2)/2. \quad (45)$$

which is R298 in (28).

So one can see that R297 is the difference in the channels gains from 30-dB couplers to RVP8 and R298 is the difference between the channel gains in the Power Sense plus Receiver. R297 is the difference in the H – V CW test signal power. R298 is a difference in channel gain from the H and V 30dB coupler to the common-circuit portion of the 'Power Sense' (just before the delay line).

2.6. Suncheck measurements.

Calibration using the solar flux is described in section 5.17.3.11 (page 5-225); the output from Subtest 3 is used for Z_{DR} calibration. There is no description on how sun measurements are used for obtaining the system Z_{DR} offset, i.e., how SMB in (1) is obtained. The following is a possible explanation.

Rationale. All measurements described in sections 2.1 – 2.5 above calibrate the signal gains in the polarimetric channels from the 30-dB couplers in RF Pallet to processor RVP8. The part of the system from the 30-dB couplers to the feed-horn and antenna was out of calibrations so far. To close the loop, the solar measurements are used. It is assumed that the Sun is unpolarized radiation source, i.e., the powers of solar flux measured in the horizontal and vertical channels are equal in the mean.

The Suncheck measurements are conducted with the antenna oriented at the Sun's center. The signal path in the horizontal channel is shown in Fig. 2.12 with the thick blue line. The gains/losses in the antenna, feedhorn and the part of the waveguides from the feedhorn to the 30-dB coupler is denoted as L_{HA}. The losses from this coupler down to the Receiver have been denoted as L_{H1} in the previous subsection. If Ps is the power of solar radiation at the input to the antenna, then power Psh measured with RVP8 in the horizontal channels is

$$Psh = Ps + L_{HA} + L_{H1} + Rrh. \quad (46)$$

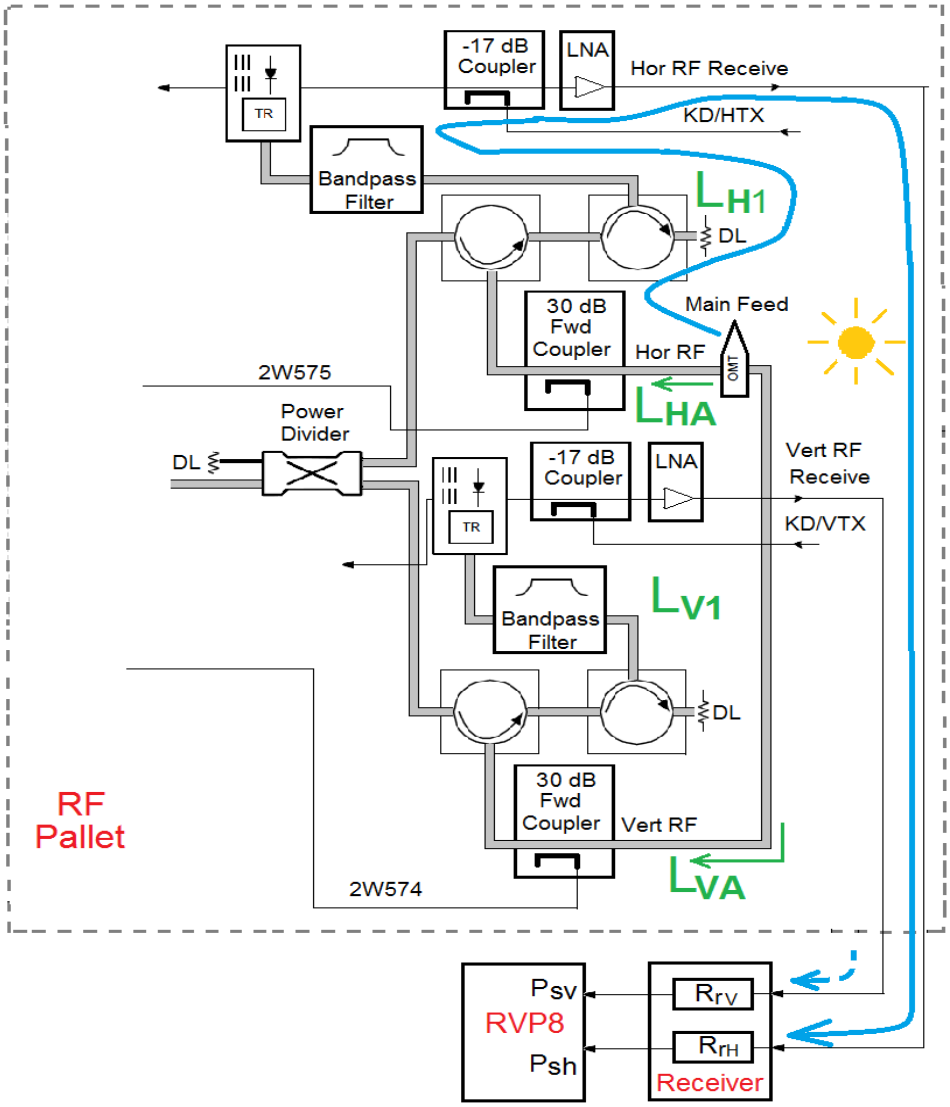

Fig. 2.12. Diagram for the Suncheck measurements.

For the vertical channel, a similar equation can be written

$$Psv = Ps + L_{VA} + L_{V1} + Rrv. \quad (47)$$

The difference $L_{HA} - L_{VA}$ can be obtained from (46) and (47)

$$L_{HA} - L_{VA} = Psh - Psv - L_{H1} - RrH + L_{V1} + RrV = Psh - Psv - RCB, \quad (48)$$

Where RCB is called by the contractor as Receiver Bias,

$$RCB = L_{H1} + RrH - L_{V1} - RrV, \quad (49)$$

which is the channel differential gain from the 30-db couplers to RVP8.

2.7. Obtaining the system Z_{DR}

The system Z_{DR} offset is obtained as

$$Z_{DR} \text{ offset} = 2^* \text{ SMB} + \text{RCB} + \text{TXB}. \quad (50)$$

(which is eq. (1) and written herein for convenience) where (Robert Macemon, the Baron, personal communication, 2013)

$$\text{SMB} = (\text{Hsun} - \text{Vsun}) - \text{RCB}, \quad (51)$$

$$\text{RCB} = (\text{Hpow} - \text{Vpow}) - \text{R297} - (\text{R293} - \text{R294}), \quad (52)$$

$$\text{TXB} = (\text{Hps} - \text{Vps}) - \text{R298} - (\text{R295} - \text{R296}), \quad (53)$$

where the measured powers and Rs are listed in table 2.

Table 2. Quantities needed to calculate the system Z_{DR}.

Quantity	How it is measured/obtained	KOUN's value, dB
Hsun	Power in the horizontal channel at IFD in the Suncheck measurements	
Vsun	Power in the vertical channel at IFD in the Suncheck measurements	
Hpow	Power in the horizontal channel at IFD while injecting CW test signal	
Vpow	Power in the vertical channel at IFD while injecting CW test signal	
R297	AME test signal bias, see section 2.5	-0.10
R293	H Coupler Test Signal Loss, factory measured	-30.20
R294	V Coupler Test Signal Loss, factory measured	-30.36
Hps	TX Horizontal Pulse Peak Power read at IFD while injecting transmitter	
Vps	TX Vertical Pulse Peak Power read at IFD while injecting transmitter	
R298	Power Sense Calibration Offset Bias, see section 2.5	-0.13
R295	H Coupler Transmitter Loss, factory measured	-30.14
R296	V Coupler Transmitter Loss, factory measured	-30.31

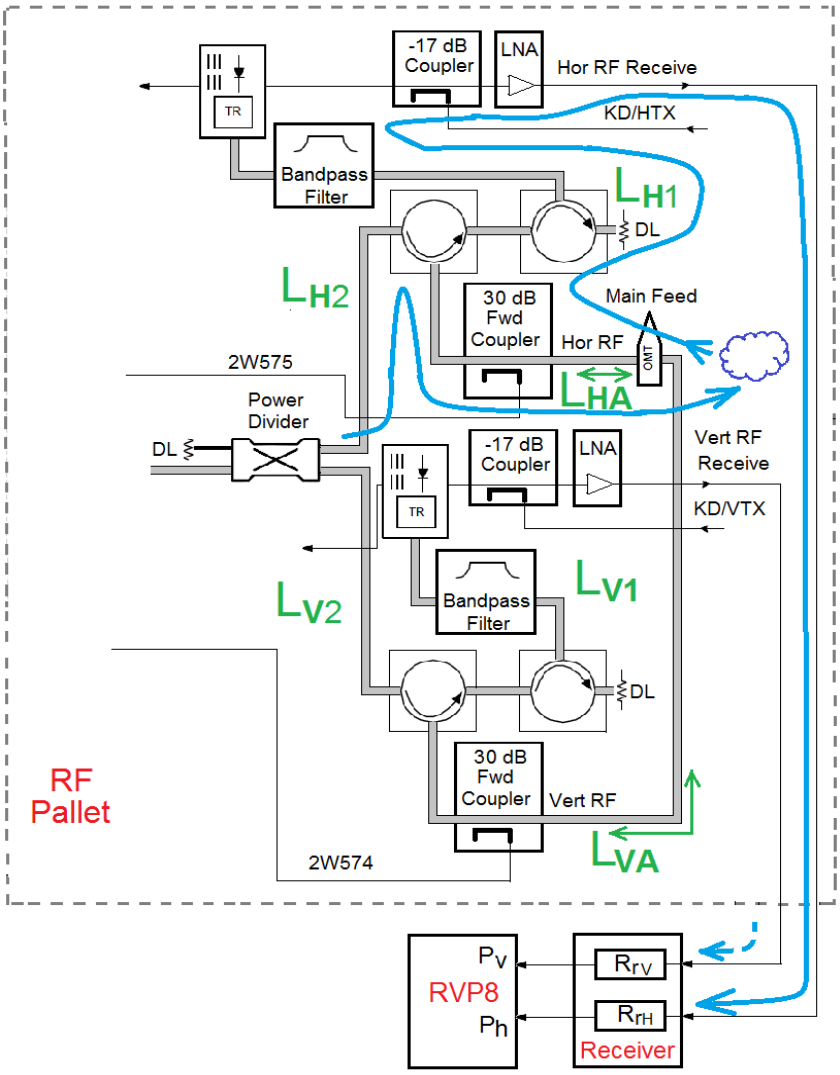

Fig. 2.13. Diagram for the system Z_{DR} calculations.

Rationale. Since there is no description of calculations (50)-(53) in the document, consider possible justifications of the calculations. Let P_H and Pv be the powers at the output from the power divider, L_{H2} is the loss from the divider's output to the 30-dB coupler and L_{HA} is the loss from the coupler to radome (Fig. 2.13).

The transmitted power P_{TH} in the H channel is

$$P_{TH} = P_H + L_{H2} + L_{HA} . \qquad (54)$$

For the vertical channel, the transmitted power P_{TV} is

$$P_{TV} = P_V + L_{V2} + L_{VA} . \quad (55)$$

The power difference $P_{TH} - P_{TV}$ in dB remains the same after scattering by weather objects with differential reflectivity of zero dB. For target's differential reflectivity of Z_{DR}, the difference in returned power is $P_{TH} - P_{TV} + Z_{DR}$. This difference is amplified by the system by $(L_{HA} + Lh_1 + Rrh) - (L_{VA} + L_{V1} + Rrv)$ and measured Z_{DRm} is

$$Z_{DRm} = P_{TH} - P_{TV} + Z_{DR} + (L_{HA} + Lh_1 + Rrh) - (L_{VA} + L_{V1} + Rrv). \quad (56)$$

But $(Lh_1 + Rrh) - (L_{V1} + Rrv) = RCB$ according to (49), thus

$$Z_{DRm} = Z_{DR} + P_{TH} - P_{TV} + L_{HA} - L_{VA} + RCB. \quad (57)$$

The system measures the difference between the transmitted powers by using the Power Sense measurements (see (36) and (37)). In notations of (53), (36) and (37) are written as,

$$Hps = P_{TH} + L_{H}2 + R293 + Rpsh + Rr_H, \quad (58)$$

$$Vps = P_{T}v + Lv2 + R294 + Rpsv + Rrv. \quad (59)$$

Obtain $P_{TH} - P_{T}v$ from the latter and substitute it into (57) with the use of (45)

$$Z_{DRm} = Z_{DR} + Hps - Vps + 2(L_{HA} - L_{VA}) + L_{H2} – L_{V2} + R294 – R293 – R298 + RCB. \quad (60)$$

Denoting

$$R295 = R293 + L_{H2,} \quad (61)$$

$$R296 = R294 + Lv_{2,} \quad (62)$$

we get

$$Z_{DRm} = Z_{DR} + Hps - Vps + 2(L_{HA} - L_{VA}) + R296 – R295 – R298 + RCB. \quad (63)$$

The system calibrates its receive paths by injecting the test signals into the coupled ports of 30-dB couplers. In notations of (52), the measured by RVP8 power difference is (see (34) and (35))

$$Hpow = R34 + R293 + Lh1 + Rr_H, \quad (64)$$

$$Vpow = R33 + R294 + Lv1 + Rrv. \quad (65)$$

Subtracting these two with the use of (49), one gets

$$RCB = Hpow – Vpow +R297 – R293 + R294. \quad (66)$$

$L_{HA} - L_{VA}$ can be obtained from the sun measurements (see (48)). Then (63) can be represented as,

$$Z_{DRm} = Z_{DR} + Hps - Vps + 2(Psh - Psv - RCB) + R296 - R295 - R298 + RCB. \quad (67)$$

Denoting

$$TXB = Hps - Vps + R296 - R295 - R298, \quad \text{and} \quad (68)$$

$$SMB = Psh - Psv - RCB, \quad (69)$$

eq. (67) can be rewritten as,

$$Z_{DRm} = Z_{DR} + TXB + 2SMB + RCB. \quad (70)$$

The system ZDR offset is the sum of three last terms on the right side of (70), which coincides with (50).

3. Analysis of the baseline Z_{DR} calibration

It follows from (70) that the system Z_{DR} offset is obtained from measurements of the transmit and receive biases and suncheck measurements. Parameters used in calculations of the system Z_{DR} offset are gathered in Table 3.

Table 3. Parameters needed for obtaining the system Z_{DR} offset

Component in the system Z_{DR} offset	Parameter	How it is measured
RCB	Hpow, Vpow	Routine receive measurements using CW calibrated signals
	R293, R294	Factory measured
	R297	Cross-and-straight measurements
TXB	Hps, Vps	Routine power sense measurements
	R295, R296	Factory measured
	R298	Cross-and-straight measurements
SMB	Psh, Psv	Suncheck measurements
	RCB	See the first table entry

RCB is the channel gain difference in a system part from the 30-dB couplers to processor RVP8. TXB is the transmit pulse power level difference injected into the antenna (sampled at the 30-dB couplers WG. SMB is the channel gain difference in a system part from the radome + antenna to the 30-dB couplers. It is seen from the Table 3 that to obtain the system Z_{DR} offset, two measurements from the calibration routines per section 2 are used: the cross-and-straight and suncheck measurements.

3.1. RCB measurements

RCB bias is obtained from the cross-and-straight measurements (section 2.5) and factory measured R293 and R294 which are the losses of 30-dB couplers to the coupler ports. The cross-and-straight measurements are manual procedures prone to errors. It is desirable to modify these measurements (see section 3.5) in order to eliminate manual connecting/disconnecting of 2W574/2W575 cables.

It is also desirable to eliminate the use of R293 and R294, i.e., factory measured quantitates because these measurements can contain uncertainties. The latter have not been indicated in the document. Some proposition on simplification of RCB measurements can be found in section 3.5.

There is a possible weak link in the RCB measurement. Injection on the calibrated signals from the built-in CW generator is done with the transmitter switched off. The regular radar observations are conducted with transmitters on. The transmit pulses warm up the circulators connected to the outputs of power divider. These circulators are in the receive circuits as well. Warm and cold circulators can have different insertion losses. So it might be desirable to measure RCB with the transmitter on to be at a radar state close to regular observations.

3.2. TXB measurements

The TXB measurement is the most vulnerable procedure in the Z_{DR} calibration. The dynamic power splitter, used in the system, requires measurements of relative powers in the channels at the divider's output. One of the possible solutions to make the TXB bias less dependent upon mechanical movement of the divider's plunger is to fix its position for a long time and use measured TXB bias throughout this time without moving the divider's plunger. The power divider does not move or automatically re-adjust operationally. Most radars are likely at the same position as left by the Dual Pol Installation. Movement of the plunger is only possible with off-line maintenance routines. The systems show time variations in TXB at the fixed plungers that signify power sense circuitry time variations. These variations could also be a result of variations of the split ratio in the divider.

3.3. SMB measurements

SMB is the difference in channel gains from the antenna + radome to the 30-dB couplers in RF Pallet. SMB should be long-time stable because these circuits contain waveguides, the metal antenna, and radome. Theoretically, only large temperature variations could change SMB but the value of such changes is unknown. So SMB measurements should be taken rarely (once in a quarter?).

There are two possible sources of errors in the SMB measurements. The first could arise from the suncheck measurements taken with the transmitter off. As it was discussed in section 3.1, this cools the circulators. Cool circulators have different insertion losses than warm circulators. To evaluate this effect, the sunchek measurements should be conducted with the transmitter on and off. This will limit available distance with available solar signals due to ground clutter up to distances of about 30 km. But this does not look substantial for the suncheck measurements because the total number of available range gates will be about 500.

The second possible source of errors is the assumption that the channel gains for wideband signals from the Sun and narrowband signals from the calibration signals are equal. This assumes that the characteristics of the first LNAs , first mixers, and narrow-band digital filters in the channels are the same for wide-band and narrow-band signals. This assumption requires direct verifications in at least three radars. Such a verification should be done by splitting the power from the CW external generator and injecting into the coupled ports of 30-dB couplers in RF Pallet. Then the same splitter should be used with the noise generator.

3.4. Linearity of the receive circuits

The baseline Z_{DR} system calibration assumes that linarites of the horizontal and vertical channels are equal. Linearity of the system is determined by the first LNAs in the channels (Fig. 3.1). According to the LNA's specs, their linearity is not worse than 0.5 dB across the dynamic range. This accuracy, i.e., 0.5 dB, is sufficient for reflectivity calibration because reflectivity is measured in the WSR-88Ds with this accuracy, i.e., with this uncertainty in representation/ quantization. For Z_{DR} measurements, this accuracy is not sufficient and linarites of the receivers must be measured and then accounted for.

To measure linearity of the radar receivers, the snap connectors on the 30-dB couplers of RF Pallet are disconnected and an external CW calibrated generator was connected to the coupler ports as it is shown in Fig. 3.2. Firstly, the CW generator was set off and the noise levels N_h and N_v in the channels were measured. Time-series signals in the radial are recorded with the RVP8. Then the measured noise powers are used to calculate all polarimetric parameters as follows,

$$Z_{DR} = 10 \log[(<P_h> - N_h)/(<P_v> - N_v)] \ \text{(dB)},$$

$$R_{hv} = <E_h^* E_v> , \qquad \Phi_{dp} = 180 \arg(R_{hv})/\pi \ \text{(deg)}, \qquad \rho_{hv} = |R_{hv}|/[(<P_h> - N_h)(<P_v> - N_v)]^{1/2},$$

where $<P_{h,v}>$ are the measured powers in the channels, the brackets stand for time averaging, $E_{h,v}$ are voltages in the channels, and the star denotes complex conjugate. Powers $<P_{h,v}>$ have been changed by injecting signal od different powers, i.e., from very weak to strong signals to cover the whole dynamic range of the radar receivers.

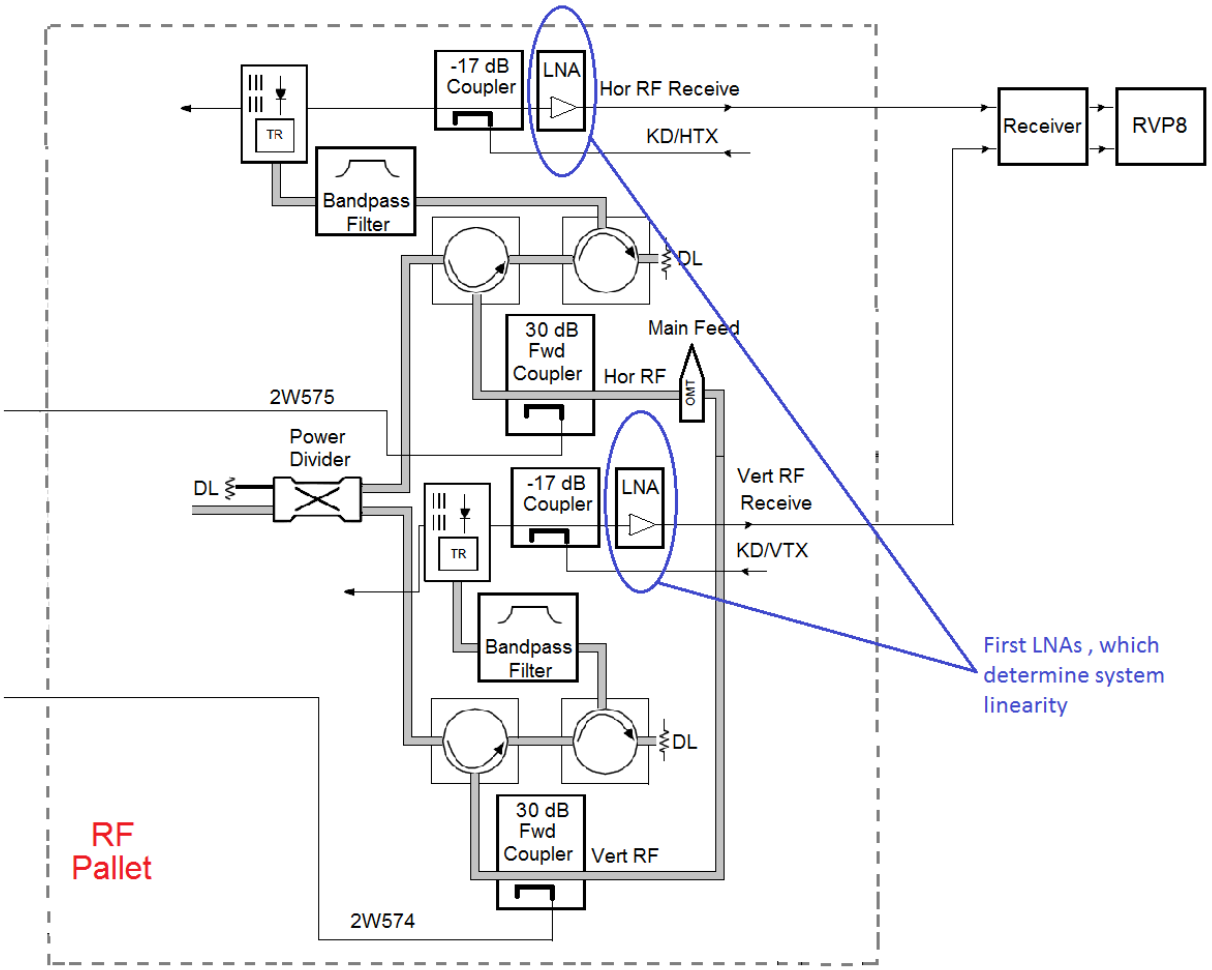

Fig. 3.1. The first LNAs in the horizontal and vertical channels (in blue ovals), which determine system linearity in Z_{DR} measurements.

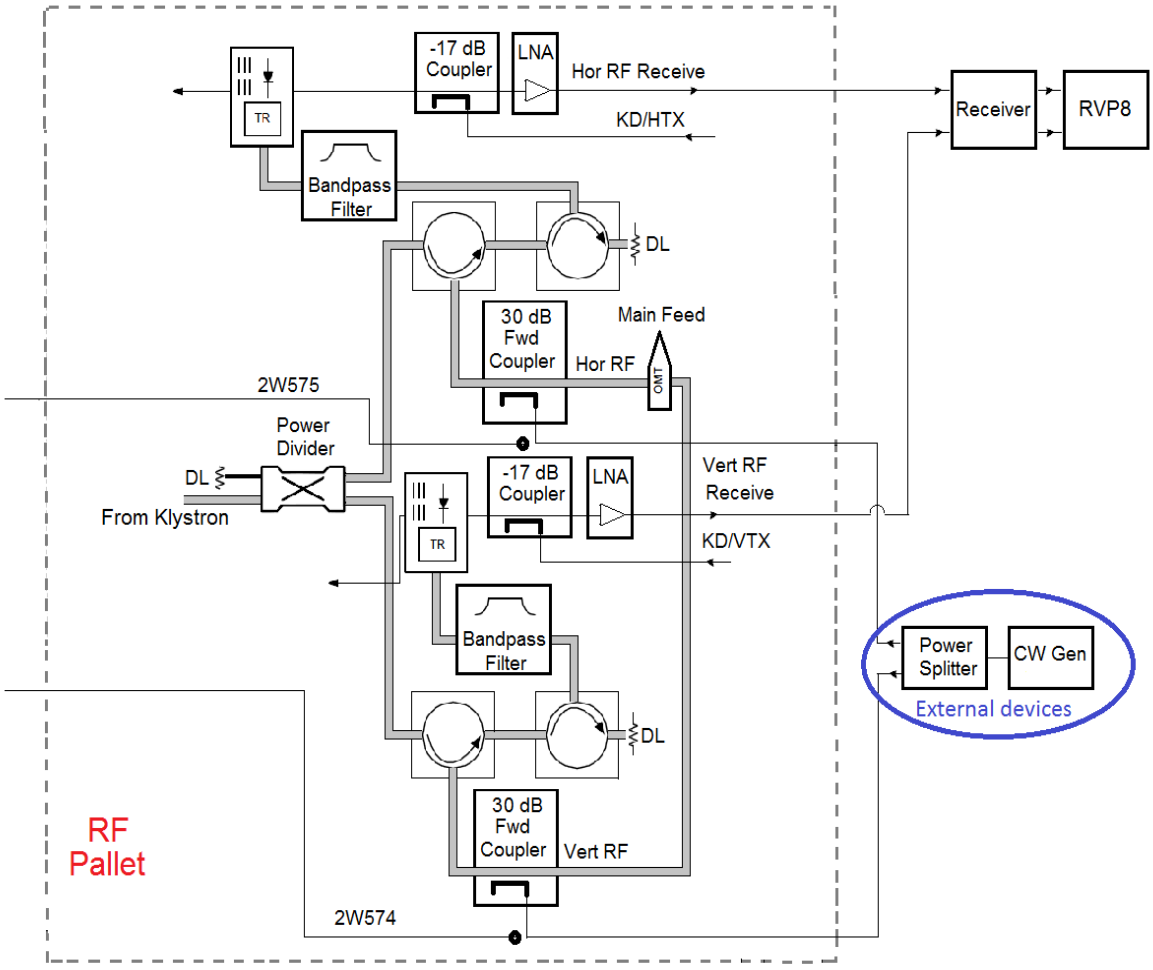

Fig. 3.2. Measurement set-up. The external CW generator, power splitter, and connecting cables are shown in the blue oval.

An example of measurement results is shown in Fig. 3.3. One can see from Fig. 3.3a that the channels are linear enough in powers so that the LNAs are good for reflectivity measurements. Radar moments are calculated in the WSR-88Ds for signals with SNR larger than 2 dB. This signal level is shown in Fig. 3.3 with the vertical dashed magenta line. So we are interested in results that are to the right of this line.

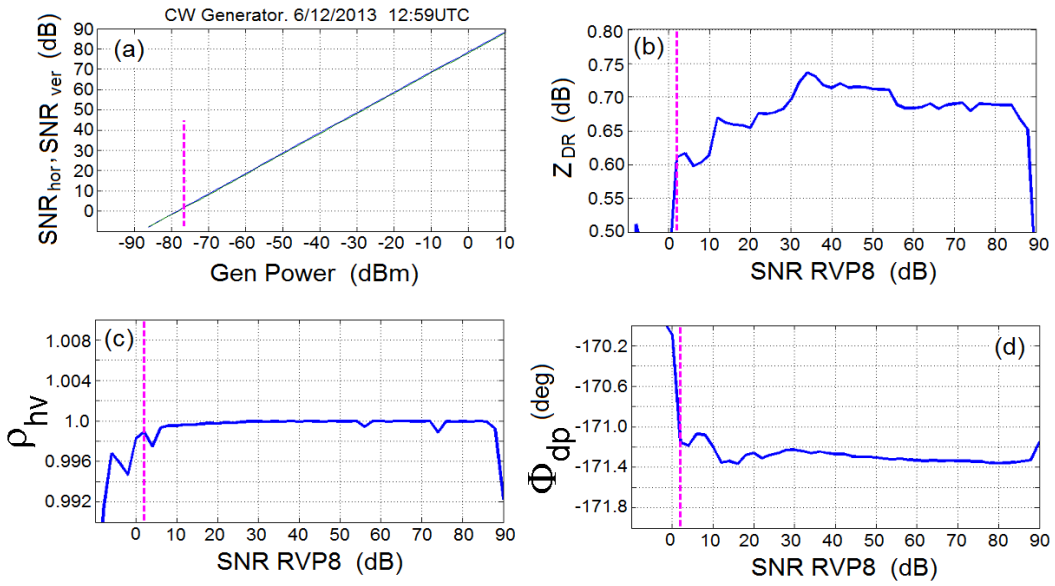

Fig. 3.3. The measured (a) power, (b) Z_{DR}, (c) correlation coefficient ρ_{hv}, and (d) differential phase Φ_{dp} on 12 June 2013 in KOUN. The vertical dashed magenta line indicates SNR = 2 dB that is used as a minimal threshold for measurements in the WSR-88Ds.

A linear Z_{DR} characteristic of the system would show up in Fig. 3.3b as a straight horizontal line. One can see that this is not the case in KOUN: Z_{DR} changes by almost 0.15 dB across the whole dynamic range. The curve has a maximum at SNR= 34 dB. At very strong signals (SNR > 88 dB), Z_{DR} drops significantly. We could not make measurements above SNR = 90 dB due to lack of generator power so about 10 dB of the upper part of dynamic range was not covered in our measurements (the dynamic range of the WSR-88Ds is claimed to be about 100 dB long pulse, 93dB short pulse). The values of correlation coefficient were very high during these measurements (Fig. 3.3c). The differential phase changes by about 0.5^{o} (Fig. 3.3d).

The results of measurements in June and July, 2013 are shown in Fig. 3.4; the measurement results for different days are shown with different colors. One can see that the shape of curves remains the same for SNR > 20 dB. The vertical shifts of the curves results from imperfect snap connectors that are discussed in section 3.5. It is seen that the curves exhibit Z_{DR} nonlinearities of 0.15 dB (Fig. 3.4a) that should be accounted for in Z_{DR} calibration. The origin of large variations in Z_{DR} at SNR < 20 dB is unknown and needs to be studied further.

The scatter in Φ_{dp} (Fig. 3.4b) at SNR > 15 dB is explained with imperfections of the snap contacts (section 3.5), but the origin of Φ_{dp} scatter at SNR < 15 dB is not known. It would be informative to make similar measurements in some other WSR-88D and compare the results.

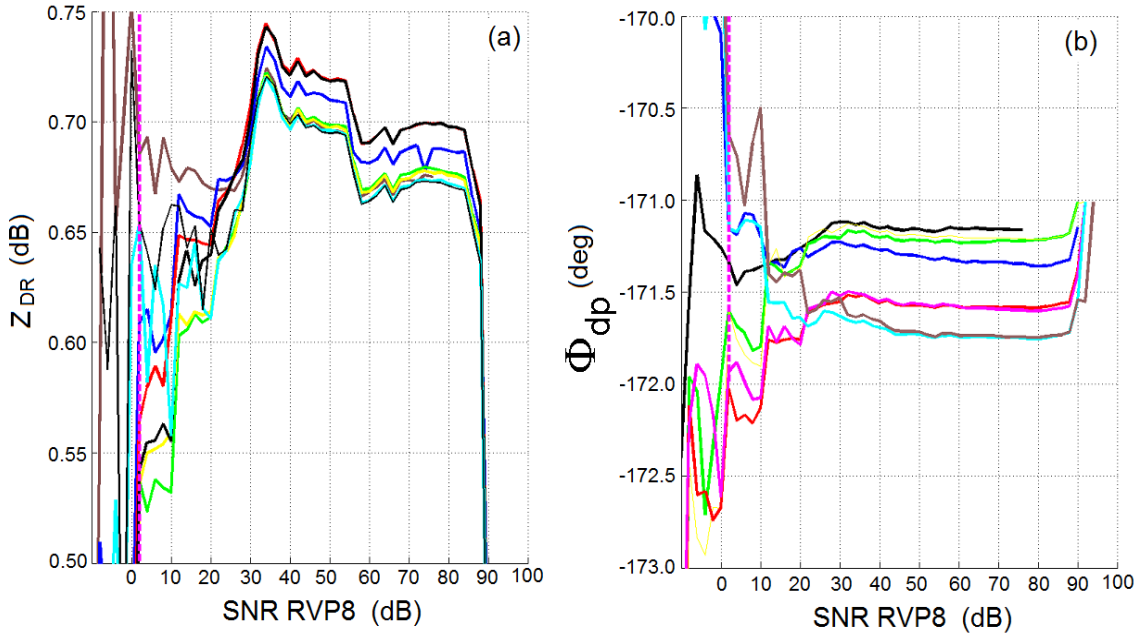

Fig. 3.4. Z_{DR} and differential phase Φ_{dp} for the measurements in KOUN. The measurement results on different days indicated with different colors.

Some measurements have been made close in time; an example is shown in Fig. 3.5 with a time delay of 15 min between the measurements (the blue and red curves). It is seen that at SNR > 15 dB in KOUN, the curves practically repeat each other but at lower SNR deviations are evident. In KTLX, the results are repeatable for SNR > 2 dB, i.e., for the whole dynamic range. The KTLX's Z_{DR} dynamic range is not linear but it deviates from the linearity by less than ±0.04 dB and this nonlinearity should be accounted for in Z_{DR} calibration.. Nonetheless, the difference in the linearity between KOUN and KTLX is alarming and there is no telling if much worst characteristic appears on some other radars. This should be checked on radars that have notoriously large Z_{DR} bias. In search of bias cause, examination of many different radars by ROC revealed that sun's measurements are one weak link prone to errors. Thus the Z_{DR} transfer function and the position of sun's SNR on it need to be evaluated for radars with large bias. Thorough analysis of the sun scan procedure is suggested. Cases of large bias should be documented and analyzed to identify the flaw(s) come up with robust solutions

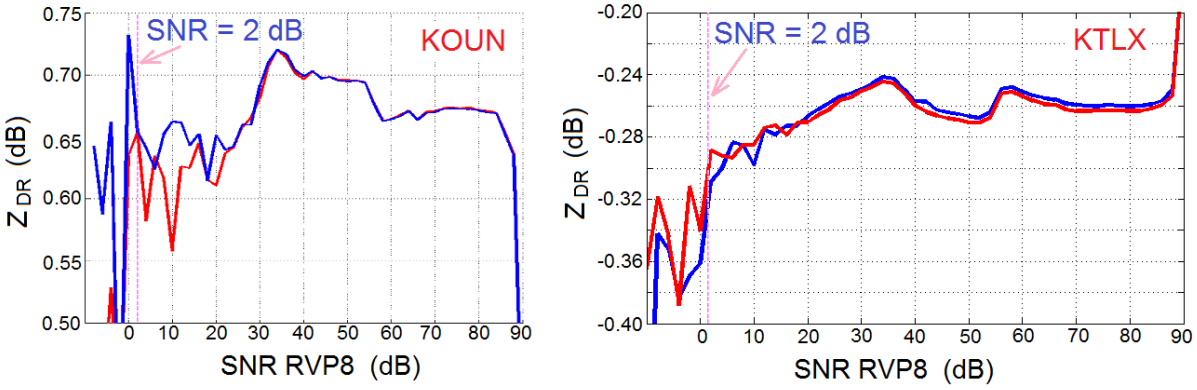

Fig. 3.5. Z_{DR} across the dynamic range for KOUN (left) and KTLX (right, measured 21 August, 2013). The blue and red curves correspond to measurements delayed by about 15 min.

3.5. Imperfections of the snap connectors in the RF Pallet

Snap connectors are used to connect 2W574 and 2W575 cables to the RF Pallet. Such connectors are used to allow manual connect/disconnect procedures in the cross-and-straight measurements in the Z_{DR} calibration (section 2.5). During antenna movements these cables experience vibrations/shocks and the snap connectors experience different mechanical load that could result in connectivity variations. Secondly, during cross-and-straight measurements the snap connectors could change their losses due to several manual connections/disconnections.

To verify stability of the connectors, the external CW generator was used; the measurement set-up is shown in Fig. 3.2. The output generator power was set to a level that produced strong signal at RVP8 with SNR of 40 dB. Then the snap connectors were disconnected and connected back to the RF Pallet manually and the signals have been recorded with RVP8 and then processed off-line. In KOUN, there were 27 circles of connect/disconnect during four days of the measurements in June and July 2013. The results are shown in Fig. 3.6. The number of disconnect/connect is shown in the abscissa and the measured Z_{DR} and the differential phase Φ_{dp} are shown in the ordinates. The correlation coefficients remained very high (> 0.995) for all measurements (not shown).

One can see from Fig. 3.6 that Z_{DR} changes noticeably: the most frequent scatter is about 0.1 dB with two measurements of way off 0.1 dB. Z_{DR} changes with the scatter of 0.1 dB and larger should be considered as unacceptable because radars have to be calibrated with this accuracy. The best way to get rid of this uncertainty would be replacing the snap connectors with an electronic device that would make such measurements without any interference from radar technician.

As it is seen from Fig. 3.6(right), disconnect/connect affects the differential phase as well: the phase scatter is about 5^o. Such scatter is easy to measure so measurements of the differential phase can be used to monitor the losses in the snap connectors. Changes in Z_{DR} and Φ_{dp} due to disconnect/connect should be taken into considerations in interpreting the results on linearity checks presented in section 3.4.

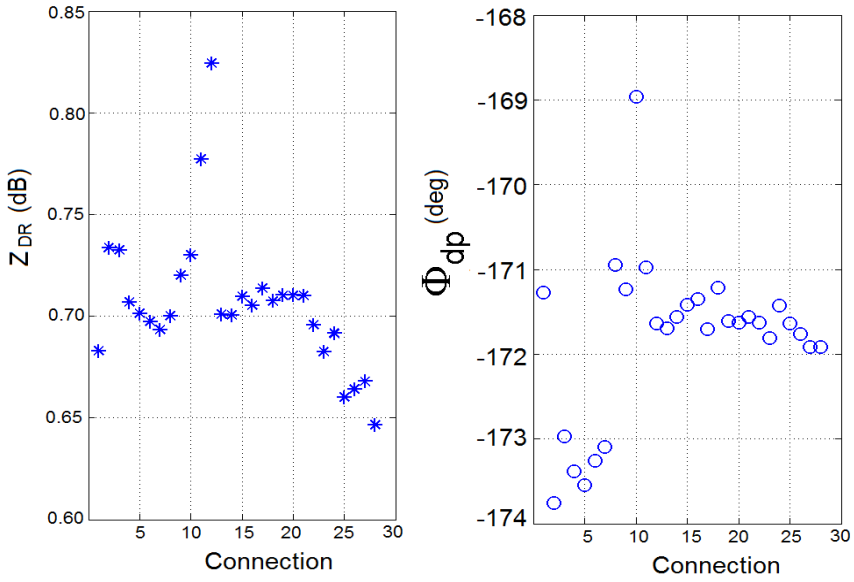

Fig. 3.6. Changes in Z_{DR} and the differential phase Φ_{dp} during disconnect/connect procedures.

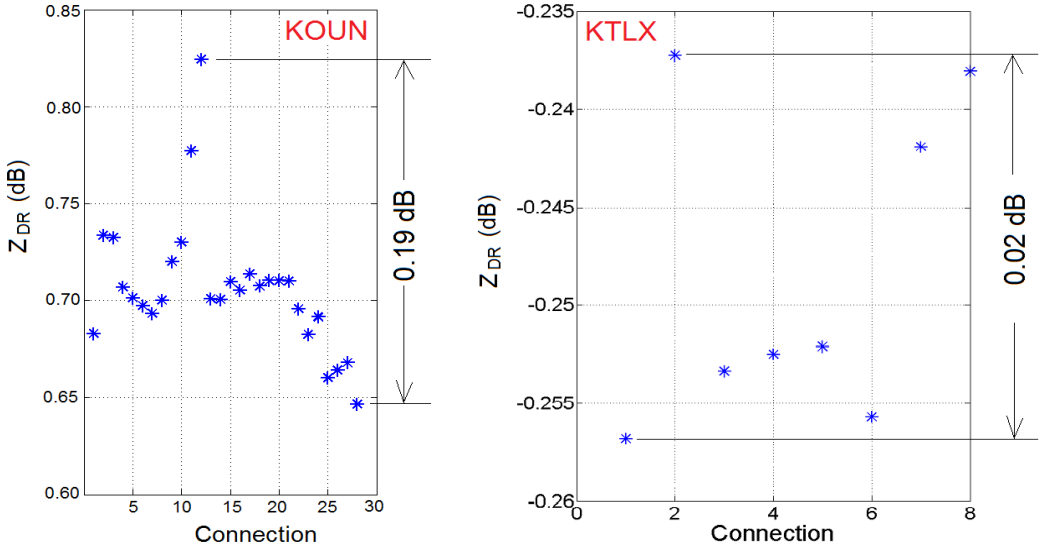

Fig. 3.7. Changes in Z_{DR} during connect/disconnect procedures for KOUN (left) and KTLX (right).

Results of Z_{DR} changes due to the disconnect/connect procedure in snap connectors for KOUN and KTLX is presented in Fig. 3.7. One can see that the maximum Z_{DR} scatter in KOUN is 0.19 dB and it is 0.02 dB in KTLX. The difference of order of magnitude looks encouraging for KTLX, but the measurements in KTLX were conducted just once (8 measurements during about 10 min) and this is not sufficient to make statistically significant conclusions. One can see that n KOUN the first 8 measurements have a small scatter comparable with that for KTLX. More measurements in KTLX are needed.

3.6. Z_{DR} difference in receive for narrow-band and wide-band signals

The RF Pallet has RF bandpass filters to suppress interference signals from other transmitters (see e.g., Fig. 3.2). RVP8 processor also has IF filters to select radar's own signals. So radar as a whole is a filter and its response can be different for narrow-band and wide-band signals. Radar transmits a narrow-band signal whereas the solar flux, which is used to calibrate Z_{DR}, is a wide-band radiation. So to correctly calibrate Z_{DR} using the solar flux, a possible Z_{DR} difference for narrow- and wide-band signals in receive should be known.

To measure this difference, set-up in Fig. 3.2 was used with two signal sources: 1) a CW Gen shown in the figure and 2) a noise generator in place of the CW Gen. The noise Gen used in the measurements had no variable power so it was connected to the coupling ports of the RF Pallet using just coax cables and a power splitter. SNR of the signal measured with RVP8 was about 23.5 dB in both channels. The same power was injected from the CW generator. Two Z_{DR} values have been measured: one is for wide-band signal (Z_{DRwb}) and the other is Z_{DR} for narrow-band signal (Z_{DRnb}). The difference in Z_{DR} has been obtained as follows:

$$\Delta Z_{DR} = Z_{DRwb} - Z_{DRnb}.$$

Table 4. Difference in Z_{DR} measured for wide-band and narrow-band signals in KOUN.

Date	06/12/13	07/08/13	07/09/13-1	07/09/13-2	07/10/13-1	07/10/13-2
ΔZ_{DR}, dB	0.044	0.082	0.089	0.081	0.075	0.075

The results are presented in Table 4. Two measurements have been made in July 9 and 10, which designated in the table with -1 and -2. It is seen that Z_{DRwb} is consistently larger than Z_{DRnb}. The results for July 2013 are consistent whereas the result in June is two times smaller. The accuracy of digital power meter is 0.02 dB. If the uncertainty of generator connectors is about the same 0.02 dB, then the July results can be considered stable. We conclude that the difference in Z_{DR}

for wide-band and narrow-band signals should be taken into account in Z_{DR} calibration using the solar flux.

The same measurements were made in KTLX on August 21, 2013. The result is $\Delta Z_{DR} = 0.02$ dB. This number is too low to affect Z_{DR} calibration. The value of ΔZ_{DR} can be frequency dependent because the filter characteristics depend upon frequency. The frequencies of KOUN and KTLX are quite different: 2705 and 2910 MHz. this issue. The values on both radars indicate that the difference between the sun's wide band and the generator's narrow band signals is an unlikely candidate for dismal Z_{DR} bias on some radars.

3.7. Possible simplifications of the RCB measurements

The cross-and straight measurements (section 2.5), that are used to obtain RCB, are manual procedures which have to be executed by well trained technicians. The procedure includes connecting/disconnecting RF cables and is prone to errors. So it is desirable to simplify the procedure and eliminate these manual operations.

Consider a possible simplification of the procedure. Obtain the RCB bias along with the suncheck measurements. Go through the following sequence of procedures. The suncheck measurements are taken first during which Psh – Psv is measured. Immediately after the suncheck measurements, signals from the built-in CW generator are injected into the horizontal and vertical channels and Hpow / Vpow are measured. The results of suncheck measurements are power Psh and Pvs which can be represented as (see (46) and (47))

$$Psh = Ps + L_{HA} + L_{H1} + Rrh. \quad (71)$$

$$Psv = Ps + L_{VA} + L_{V1} + Rrv. \quad (72)$$

By injecting signals from the built-in CW generator we measure Hpow and Vpow (see (64) and (65))

$$Hpow = R34 + R293 + Lh1 + Rr_{H}, \quad (73)$$

$$Vpow = R33 + R294 + Lv1 + Rrv. \quad (74)$$

Obtain difference $L_{H1} + Rrh – (L_{V1} + Rrv)$ from (71) and (72) and substitute it into (73) and (74):

$$Hpow – Vpow = Psh – Psv - L_{HA} + L_{VA} - R297 + R293 – R294. \quad (75)$$

The last five terms on the right hand side of (75) are constant because corresponding hardware do not contain active elements (like LNAs, receivers, etc.). So we can obtain their contributions altogether without connecting/disconnecting cables. The suncheck measurements are used just ones to relate powers Psh – Psv to current powers Hpow – Vpow from calibrated generator.

The receiver bias is determined as

$$RCB = Hpow - Vpow + R297 - R293 + R294 \quad (76)$$

so that (75) can be represented in the following form

$$RCB = Psh - Psv - L_{HA} + L_{VA.} \quad (77)$$

Thus RCB can be obtained from the suncheck measurements if $L_{HA} - L_{VA}$ is known. The latter is the differential losses of the waveguides from RF Pallet to antenna, feedhorn, and antenna. The total loses of these elements in a single channel is about 0.4 dB so that the differential losses should be a small fraction of it. It is of interest to measure $L_{HA} - L_{VA}$ in several radars. If this is small and constant for the WSR-88D, this number could be used in the radar network and RCB can be monitored using (77) which does not require connecting/disconnecting cables.

4. Verifying Z_{DR} calibration

Z_{DR} calibration procedures require verifications. Such verifications should be based on natural targets/objects with known Z_{DR}. The most trusted verification method is based on observations of raindrops with a vertically pointed antenna. Due to symmetry of raindrops seen from beneath, Z_{DR} should be close to 0 dB. This method cannot be implemented with the WSR-88D because its antenna cannot be directed vertically.

Another well-known method is based on observations of light rain. It is assumed that rain with reflectivity less than 20 dBZ contains small rain drops with Z_{DR} less than 0.2 dB. So radar observation of drizzle can be used to verify Z_{DR} calibration. The assumption that low reflectivity has low Z_{DR} is prone to errors because even light rain/drizzle can contain small number of sufficiently large drops that can bias Z_{DR} high. Nevertheless this method allows obtaining radars with "odd" system Z_{DR} and is used on the WSR-88D network.

In the next subsections, two new approaches are considered. The first one is based on observations of reflections from clear air free from precipitation and insects. Such reflections are frequently called Bragg scatter. The second approach is based on Z_{DR} measurements of the Moon. This method is discussed in subsection 4.4.

4.1. Reflection from clear air as a natural check for Z_{DR} calibration

Bragg scatter is reflection from turbulent clear air free from raindrops and insects/birds. Air eddies contributing to backscatter have sizes about half of the radar wavelength. Thus for the WSR-88Ds, these sizes are about 5 cm. It is assumed that such small eddies are homogeneous

scatterers with differential reflectivity of 0 dB. This property is attractive to be used as natural Z_{DR} calibrator.

An example of Bragg scatter in an RHI is shown in Fig. 4.1: a layer of Bragg scatter is located at heights around 2 km. Beneath this echo, at heights below 1.5 km, strong reflections from insects are apparent. The presence of Bragg scatter was confirmed with data from the NPN wind profiler located 29 km to the South from KOUN (the Purcell site). The maximal SNR in the layer of Bragg scatter reaches 20 dB and the mean Z_{DR} in echoes with SNR >10 dB is less than 0.2 dB.

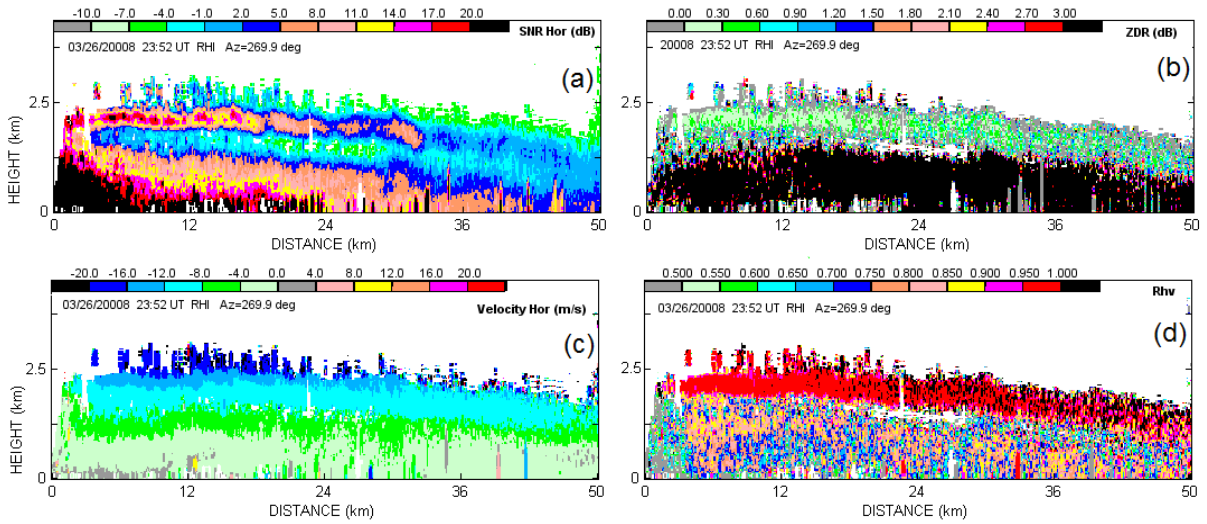

Fig. 4.1. Bragg scatter echoes at heights about 2 km observed by WSR-88D KOUN on 26 March 2008 at 2352Z at azimuth of 290^o. Vertical cross-sections (RHIs) of (a) SNR in dB, (b) Z_{DR} in dB, (c) the Doppler velocity in m s^{-1}, (d) correlation coefficient.

Examples of of Z_{DR} and the correlation coefficient histograms from Bragg scatter are shown in Fig. 4.2. The data were collected in 2008 with well calibrated WSR-88D KOUN. It is seen that the median Z_{DR} from Bragg scatter is close to 0 dB and the correlation coefficients are very high with the median values from 0.994 to 0.996. Values of the coefficients at the histograms' maximum are from 0.998 to 1.0. Such values can be used to separate Bragg scatterers from contaminating echoes of ground clutter and insects. The very right column in Fig. 4.2 represents Z_{DR} and ρ_{hv} for drizzle. It is seen than the most frequent Z_{DR} values from this drizzle was 0.22 dB, i.e., not zero, which signifies that Z_{DR} for light rain can be 0.2 – 0.3 dB depending on the relative number of large drops.

Bragg scatter is not universally suited to calibrate radar Z_{DR} because of its intermittent presence. But to check Z_{DR} calibration, Bragg scatter can be employed. This method can also be used to calibrate Z_{DR} because experiments with KOUN (section 4.2) show that sufficient Bragg scatter is

observed at least for 4-5 days in a month that is sufficient for the calibration. Bragg scatter signals have maximal SNR values of 15 – 20 dB and this level is sufficient to make reliable measurements (for instance, the solar flux produces SNR of 10 -12 dB in the WSR-88Ds). To select areas with Bragg scatter, very high values of correlation coefficients ($\rho_{hv} > 0.95$) can be used. The differential phase from areas of Bragg scatter exactly equals to the system differential phase, that can also be used for the recognition. The Z_{DR} calibration using Bragg scatter has a distinct advantage because it is applied to the receive and transmit radar circuits.

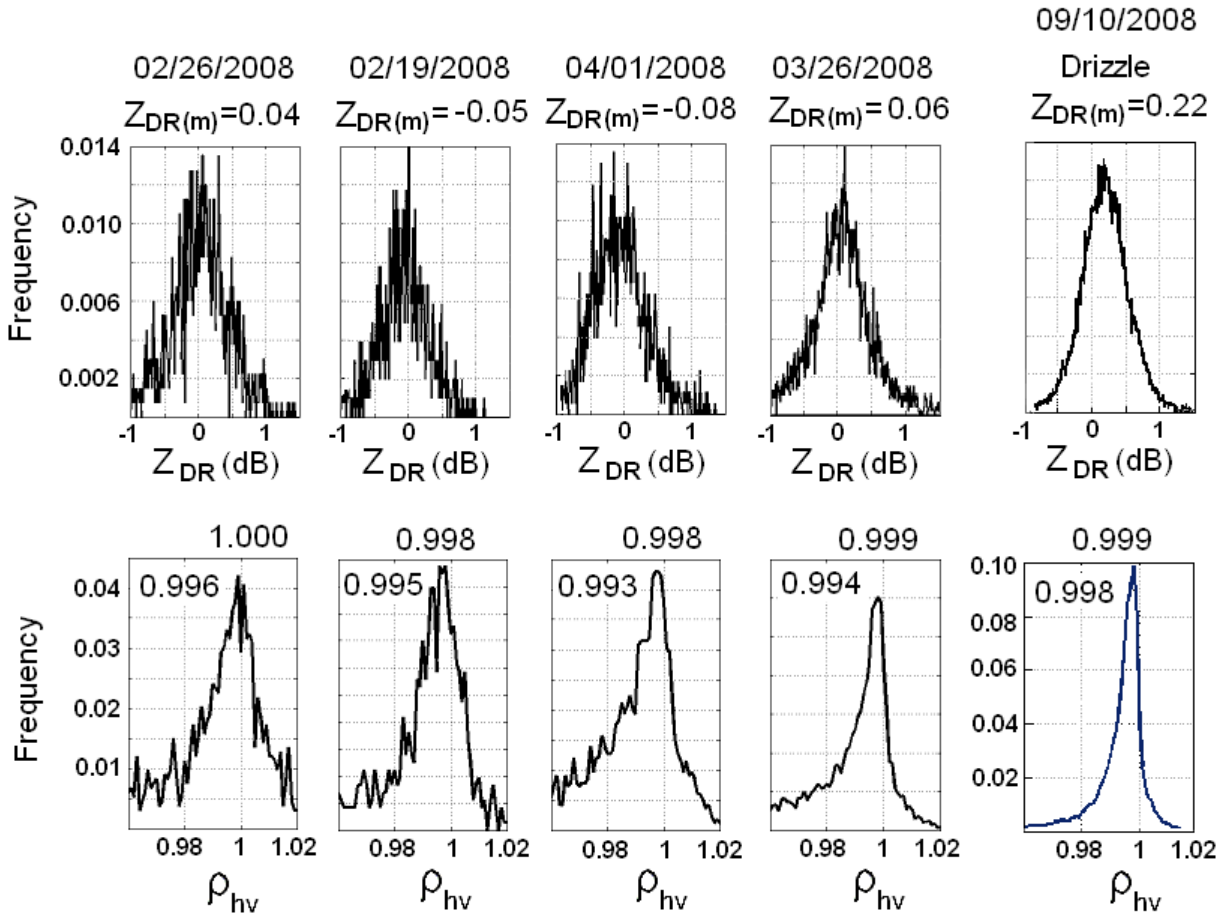

Fig. 4.2. Frequency of occurrences of Bragg scatter Z_{DR} and correlation coefficient ρ_{hv} (CC) represented in columns for each observation. The last column is for drizzle with similar signal-to-noise ratios. The top string shows heights above which the data were analyzed. $Z_{DR(m)}$ stands for the median value. Values of ρ_{hv} at the maxima of the histograms are presented at the tops of the ρ_{hv} panels, the values inside the panels stand for the median values of ρ_{hv}.

4.2. Experiments on KOUN in 2013

To establish statistics of sufficient Bragg scatter signals for Z_{DR} calibration, data from "clear air" were collected with KOUN from January to August 2013. There were five goals of these experiments:

a. What are signal-to-noise ratios from Bragg scattering to make reliable Z_{DR} measurements?
b. How often Bragg scatter is observed in central Oklahoma?
c. What are the optimal elevation angles and ranges for such observations?
d. How can Bragg scatter be separated from insects/birds' echoes and ground clutter?
e. What pulse width is preferable for the observation: short or long?

To address the above questions, a few new VCPs have been designed for KOUN. One type of VCPs was an RHI in a given azimuth. Often, Bragg scatter appears in a form of horizontal layers thus an RHI is well suited for such observations. The maximum elevation angles for RHI VCPs has been chosen to be 40^o to observe layered Bragg scatter at close distances. This angle is well above the maximum elevation angles of 20^o in the regular VCPs that are in use in the WSR-88Ds. The second type of VCPs for observations of Bragg scatter with KOUN were a PPI type VCP with arbitrary elevation angle including a very high elevation of 40^o. There is no room in this report to discuss various cases observed with the designed VCPs so several examples are presented below and some conclusions are summarized in section 4.3. Examples of data collected with the RHI and PPI VCPs are in Figs. 4.3 and 4.6. The results presented below do not represent the best time for observations of Bragg scatter.
The data were collected with KOUN, when it was available. The vast majority of the data was collected around time of 0Z to be compared with rawinsonde sounding at Norman, OK. Preferable azimuth of observation was 191^o, which is the direction of Purcell, OK, NPN wind profiler. The results are presented below from January to July 2013.

January 2013. Examples of Bragg scatter in an RHI are shown in Fig. 4.3. Panels (a,b,c) present results collected with the long radar pulse whereas results for the short pulse are shown in panels (d,e,f). One can see that the long pulse allows to observe Bragg scatter at longer distances up to 90 km but at distances within 50 km contamination from residual ground clutter is strong that causes drops in ρ_{hv} and these areas are removed by the data filter, which passed through echoes with $\rho_{hv} > 0.8$. So the long pulse is good for such observations for low Bragg scatter with altitudes below 1.0 -1.5 km. In such cases, VCP31 can also be used.

The short pulse mode (Fig. 4.3d,e,f) can be used at distances within 50 km. This pulse allows better suppression of ground clutter but SNRs are lower than those for the long pulse. Another case with the short radar pulse is shown in Fig. 4.4 with Bragg scatter located at heights between 2.2 and 2.9 km. Maximum SNR are observed between elevation angles of 5^o and 6^o.

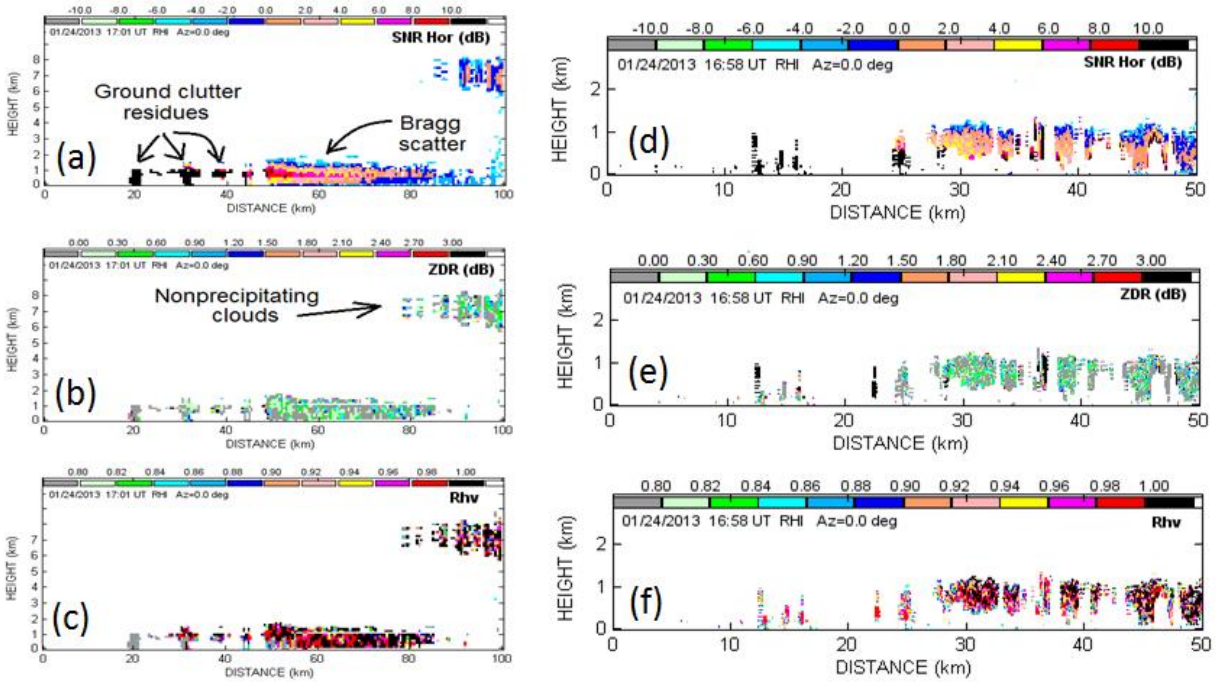

Fig. 4.3. Vertical cross sections of Bragg scatter on Jan 24, 2013 at azimuth of 0^o collected with the long radar pulse (a,b,c) and short pulse (d,e,f). The type of images is shown inside the panels. Rhv in the images stands for ρ_{hv}. The parameters of data filter: $|V| > 0.2$ m s^{-1}, $\rho_{hv} > 0.8$.

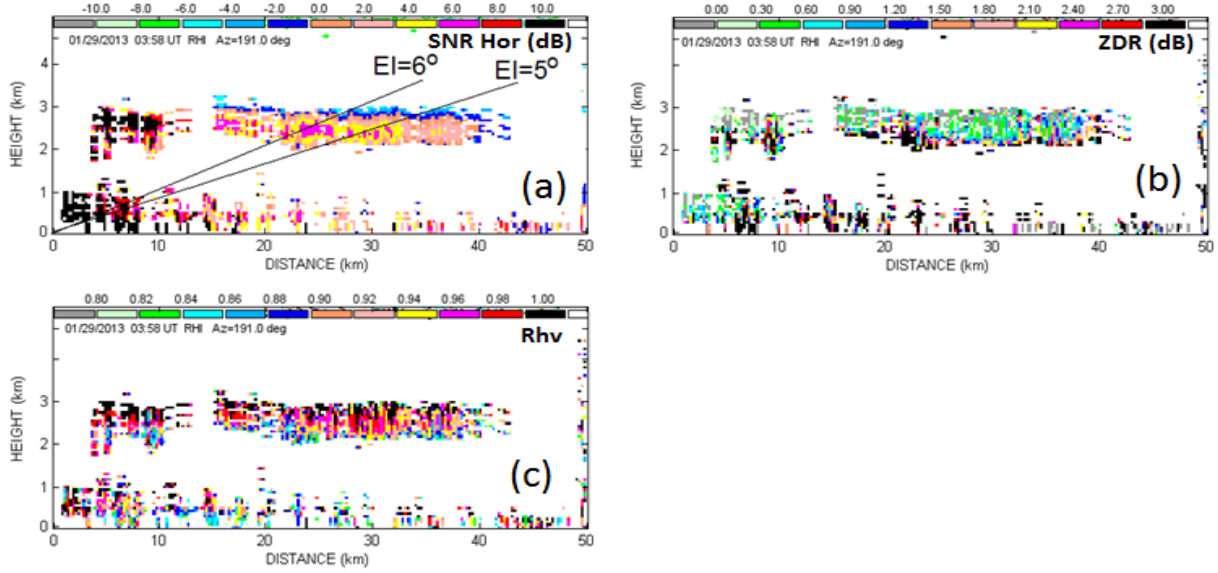

Fig. 4.4. Vertical cross sections of Bragg scatter on Jan 29, 2013 at azimuth of 191^o collected with the short radar pulse. The parameters of data filter: $|V| > 0.2$ m s^{-1}, $\rho_{hv} > 0.8$, $40^o < \Phi_{DP} < 60^o$.

February 2013. An example of observations is shown in Fig. 4.5 for the short radar pulse (panels a,b,c) and the long pulse (d,e,f). In the short pulse mode, Bragg scatter is observed well whereas in the long pulse mode, the echo is fuzzy at all distance: at short distances, contaminations from ground clutter residues are strong and at long distances, signal is weak. So in this case, observations with the short pulse are preferable. The elevation angles with strongest signals are from 2^o to 20^o.

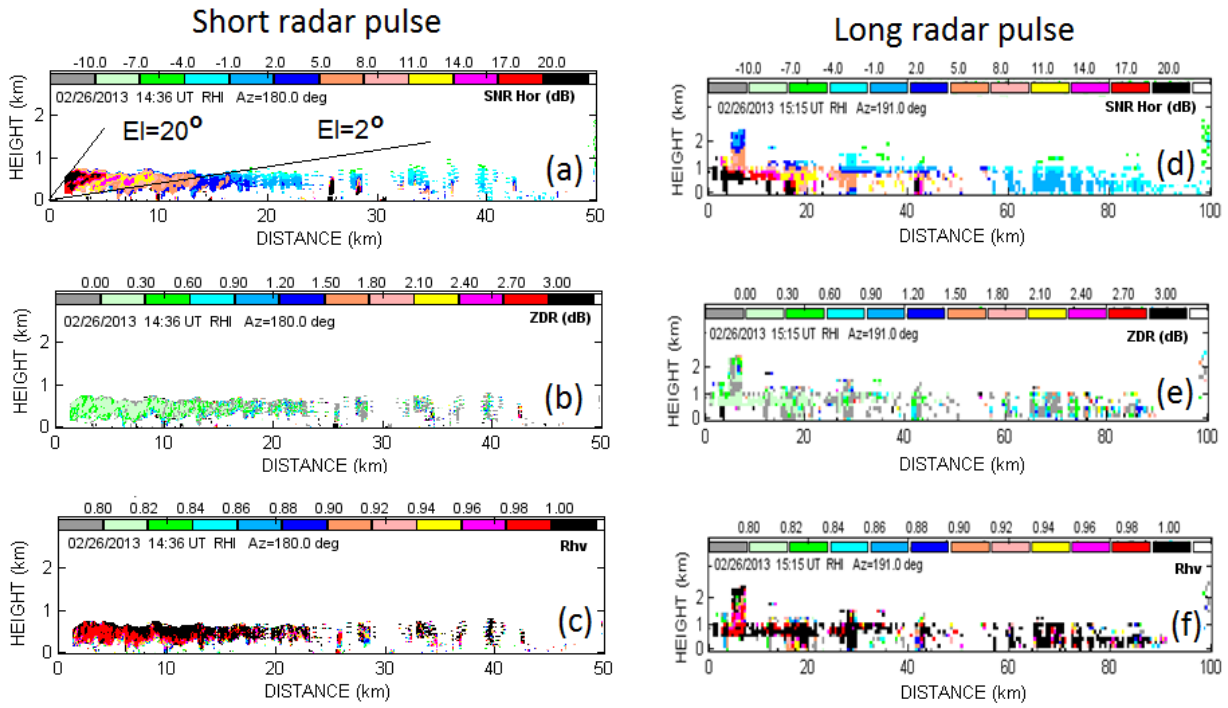

Fig. 4.5. Vertical cross sections of Bragg scatter on Feb. 26, 2013 at azimuth of 180^o collected with the short radar pulse (a,b,c) and long pulse (d,e,f). The parameters of data filter: $|V| > 0.2$ m s^{-1}, $\rho_{hv} > 0.8$.

March 2013. An example of observation with the PPI VCP is shown in Fig. 4.6. A patchy pattern is evident in the figure. Most likely, this is a manifestation of a strip structure of Bragg scatter similar to the "cloud streets". The echo patches are observed in areas where the radar beam intersects the "streets". Such cases are almost ideal for Z_{DR} calibration: the elevation angle is sufficiently high for good suppression of ground clutter and contamination from insects and birds is negligible because of the season. Two more cases are displayed in Fig. 4.7. The case on March 6 exhibits two layers of Bragg scatter. The elevation angles with strongest Bragg scatter are located between elevations of 2^o and 30^o. The latter elevation is above the maximal elevations employed with current standard WSR-88D VCPs (19.5^o) thus a special VCP could be required for optimal observations of Bragg scatter.

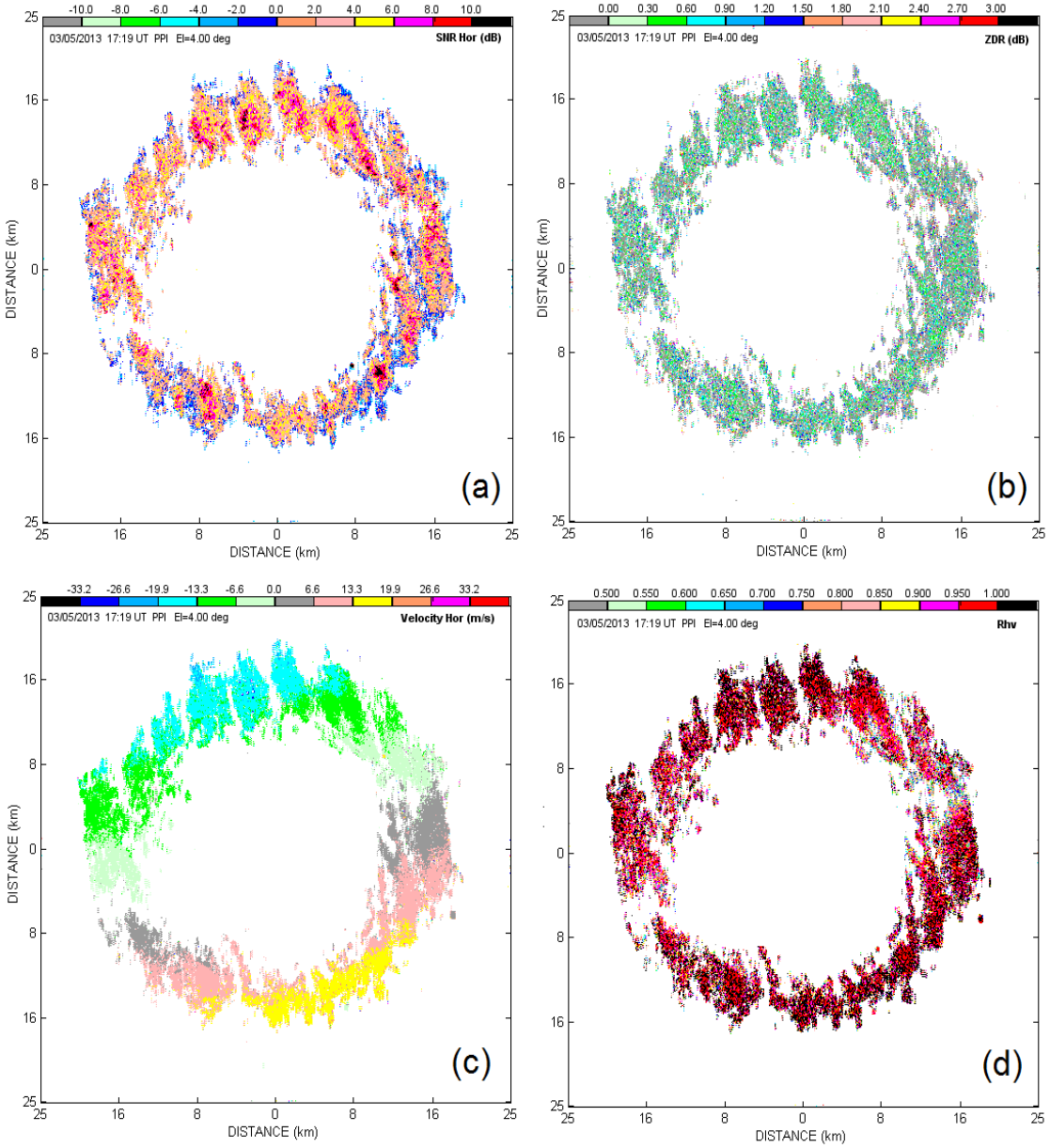

Fig. 4.6. Bragg scatter echoes observed on 5 March 2013 at 1719Z at elevation of 4^o. (a) SNR in dB, (b) Z_{DR} in dB, (c) Doppler velocity in m s^{-1}, (d) correlation coefficient. The parameters of data filter: $|V| > 0.2$ m s^{-1}, $\rho_{hv} > 0.8$.

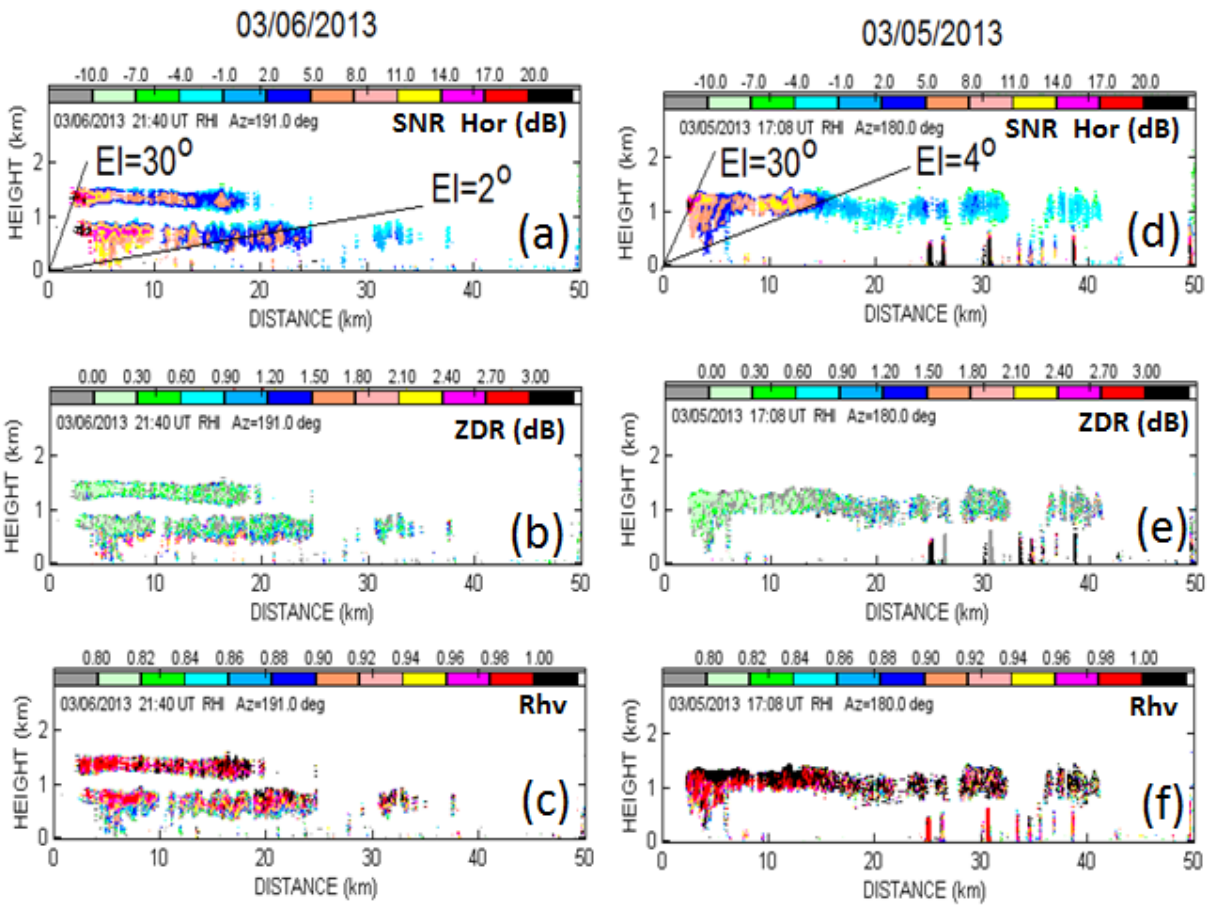

Fig. 4.7. Bragg scatter echoes observed on (a,b,c) 6 March 2013 at Az = 191° and (d,e,f) 5 March, 2013 at Az=180°. The parameters of data filter: $|V| > 0.2$ m s^{-1}, $\rho_{hv} > 0.8$.

April 2013. An example of observations is shown in Fig. 4.8. Bragg scatter was observed at heights from 1 to 2.5 km. The optimal elevation angles in this case are in an interval from 6° from 35°. The data were filtered using two thresholds: $|V| > 0.2$ m s^{-1} and $\rho_{hv} > 0.9$. The first threshold is applied to reduce the residues of ground clutter cancellation. The second one is utilized to suppress insects/birds echoes.

May 2013. An example is shown in Fig. 4.9. Bragg scatter is located at heights from 1.0 to 2.2 km. The optimal elevation angles lays in an interval from 6° to 40°.

June 2013. An example of observations is shown in Fig. 4.10. Bragg scatter is located at heights from 1 to 2 km. Echoes from nonprecipitating clouds are seen at heights from 5.7 to 8.2 km. The optimal elevation angles for observations of Bragg scatter are from 3° to 15°.

July 2013. Examples of observations are shown in Fig. 4.11. The optimal elevation angles for the observations are from 2.5° to 7° on July 19 and from 2° to 10° on July 29.

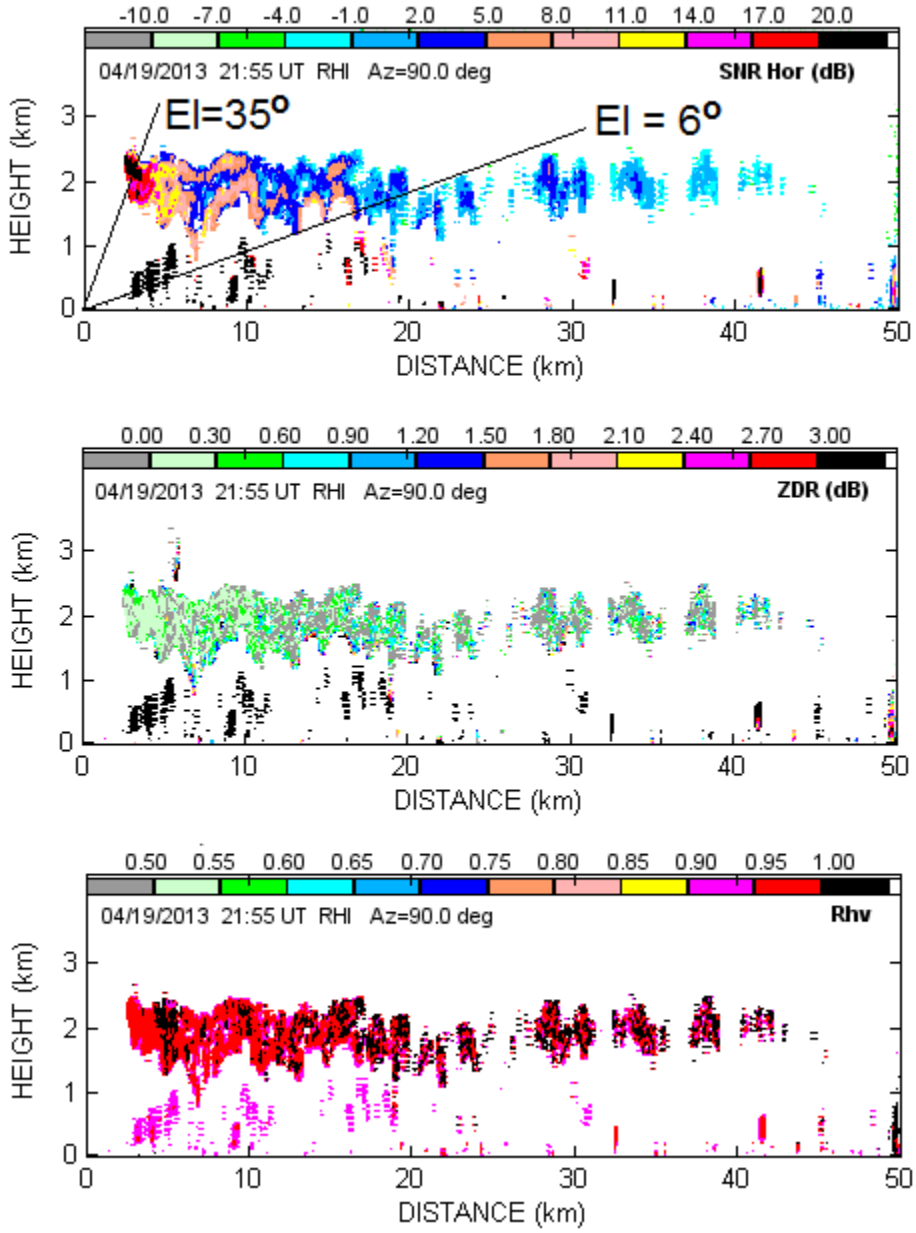

Fig. 4.8. Bragg scatter echoes observed 19 April 2013 at Az = 90°. The parameters of data filter: $|V| > 0.2$ m s^{-1}, $\rho_{hv} > 0.9$.

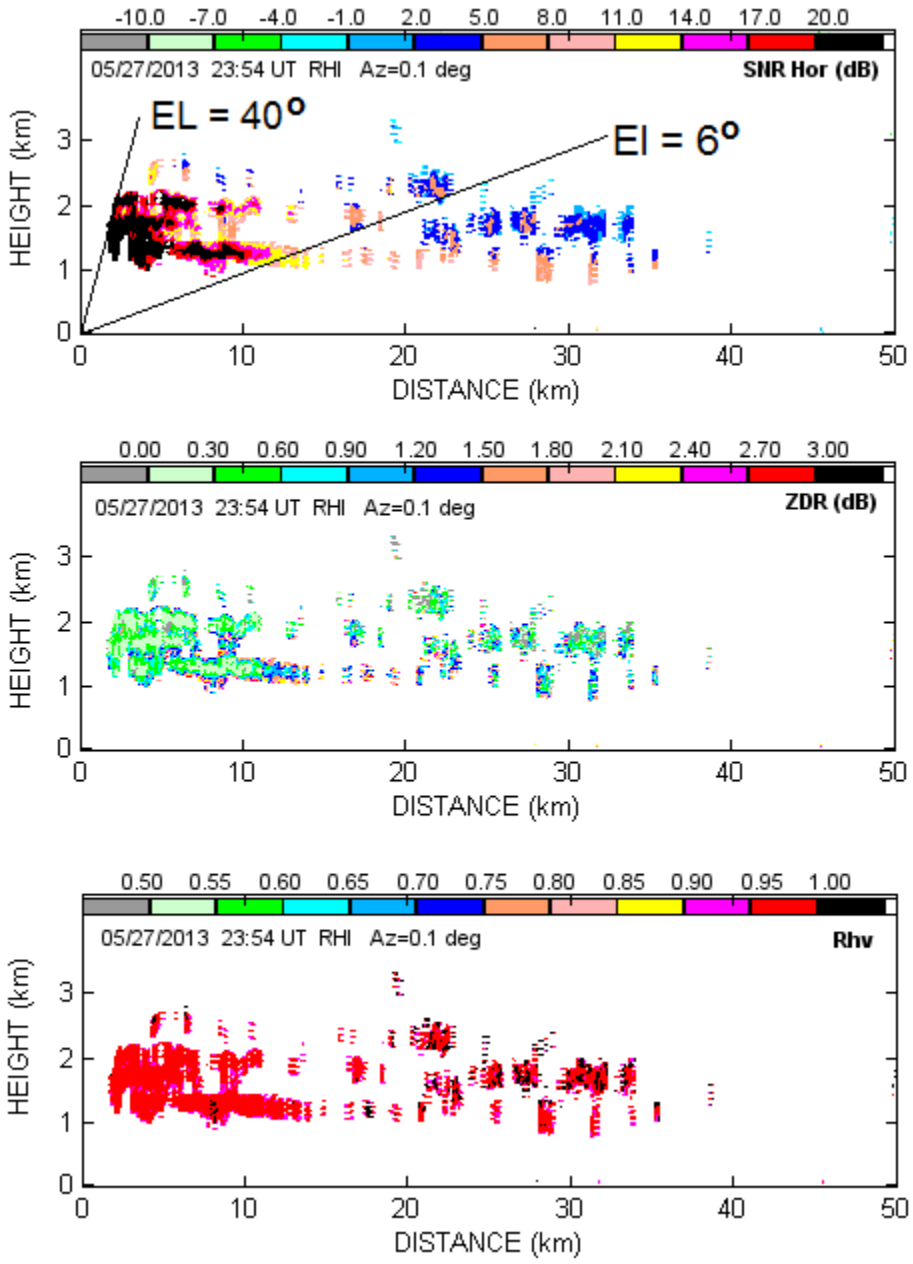

Fig. 4.9. Bragg scatter echoes observed 19 April 2013 at Az = 90°. The parameters of data filter: $|V| > 0.2$ m s^{-1}, $\rho_{hv} > 0.9$.

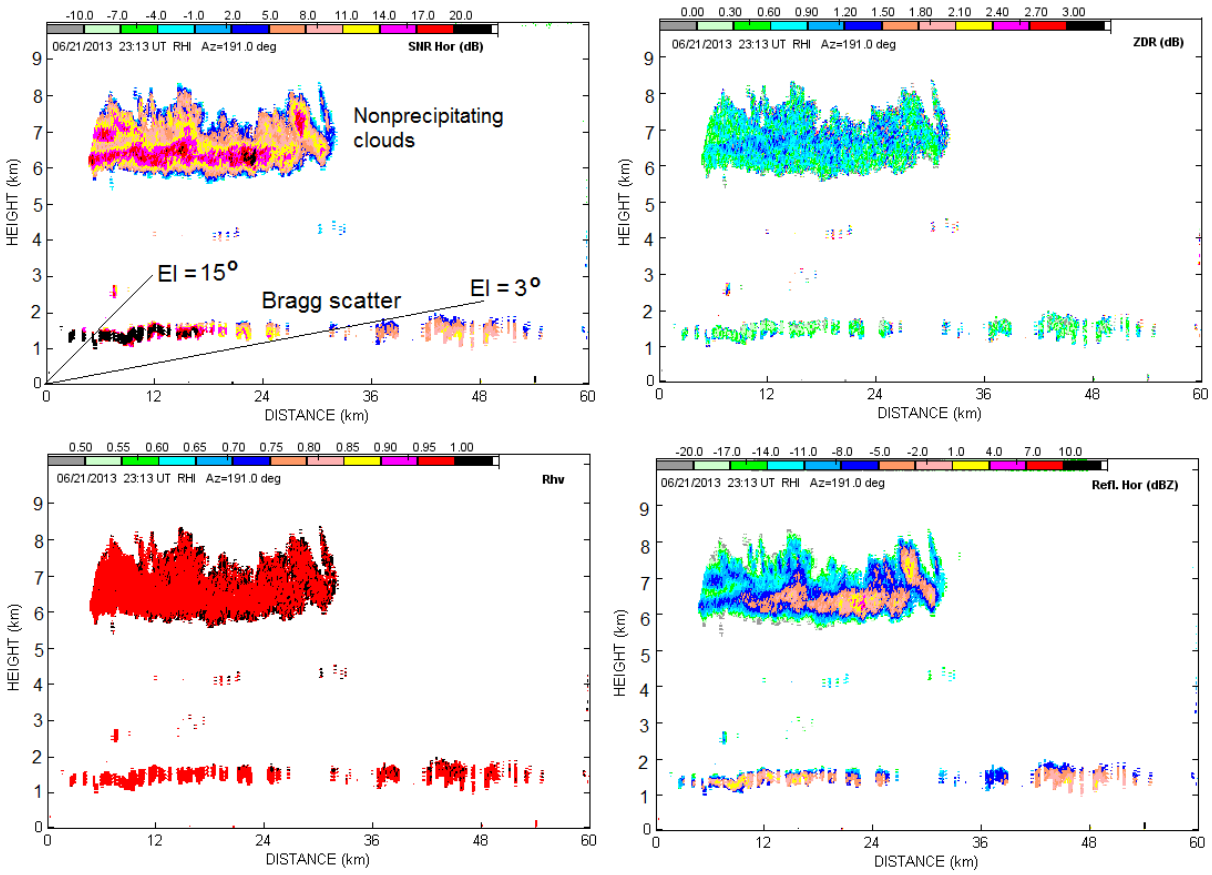

Fig. 4.10. Bragg scatter echoes observed 21 June 2013 at Az = 191°. The parameters of data filter: $|V| > 0.2$ m s^{-1}, $\rho_{hv} > 0.95$, $Z_{DR} < 3$ dB.

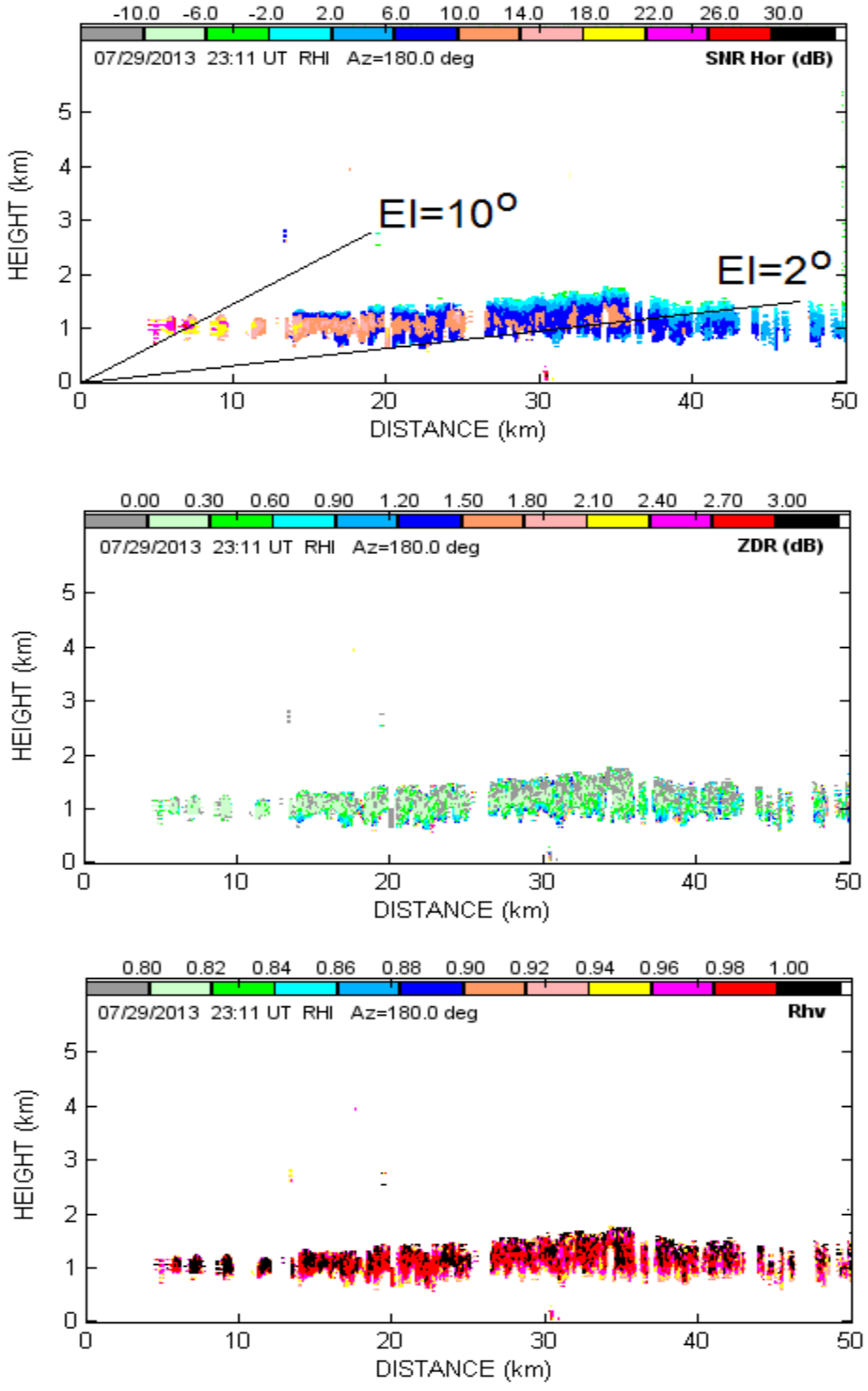

Fig. 4.11. Bragg scatter echoes observed 19 July 2013 at Az = 191°. The parameters of data filter: $|V| > 0.2$ m s^{-1}, $\rho_{hv} > 0.9$.

4.3. VCPs to observe Bragg scatter

It follows from section 4.2 that Bragg scatter echoes typically show up in a layered form. The height of such a layer plays a critical role in its radar observation. Layers with heights lower than 1.5 km are observed better with the long radar pulse. In such cases, Bragg scatter should be observed using "clear air" VCP31, which has better sensitivity than the short pulse VCPs do. At shorter distances (within 60 km) the long pulse mode suffers from ground clutter residues and utilizations of the short radar pulse is preferable.

The SNRs from Bragg scatter lay in an interval from 0 to 25 dB and, depending on the range from radar, can produce reflectivity factors from -15 to 20 dBZ. The optimal elevation angles for observations of Bragg scatter lay in a wide interval from 0.5^o to 40^o. Angle interval from 0.5^o to 4.5^o is covered with VCP31 and VCP12 covers elevations from 0.5^o to 19.5^o. Both VCPs have been successfully used to observe Bragg scatter by J. Cunningham and W. Zittel from the ROC. These two VCPs do not cover the whole interval of optimal elevations. It was demonstrated in section 4.2 that the maximum elevations reach 40^ofrequently. Natural regime of antenna movements for the WSR-88Ds is PPIs at given elevations. To cover high elevations, the following VCP can be used to observe Bragg scatter and to calibrate Z_{DR}: PPIs with 8 antenna elevations (5, 10, 15, 20, 25, 30, 35, and 40 degrees), the short pulse mode with oversampling in range should be employed. The maximal range of data collection can be limited to 70 km. Experiments with KOUN show that the short radar pulse allows for better ground cancellation and range oversampling allows obtaining more data and produce more statistically significant histograms for Z_{DR} calibration. Range oversampling is currently used in the WSR-88D for measurements of the amplitude of the burst pulse so it is not new for these radars.

4.4. Relative Z and Z_{DR} calibration using the Moon

The Moon is one of the natural objects that can be used for relative Z and Z_{DR} calibration. Z_{DR} from the Moon's surface and its persistence are not known nevertheless it is very likely that the average Z_{DR} is 0 dB. Z_{DR} measurements using the Moon could be employed for relative radar calibration. Such calibration assumes that there is at least one well-maintained and well-calibrated radar. Such radar could be WSR-88D KCRI at the Radar Operations Center. The Moon should be observed simultaneously with KCRI and other radar to be calibrated. KCRI's Z_{DR} from the Moon could be used as the true value for the second radar. To avoid possible interference between signals from two radars (if they have the same frequency) such measurements could be conducted alternatively with a small time delay between measurements.

Observations of the MOON with WSR-88D KOUN were conducted in January – March 2013. An example of signal reflected by the Moon is in Fig. 4.13 where the differential phase (Φ_{dp}) and correlation coefficient (ρ_{hv}) as functions of range are presented (the upper panel). Signal-to-nose ratios (SNR) in the polarization channels are depicted in the lower panel along with Z_{DR}. The experiments were conducted with the long radar pulse (4.5 us) at the radar pulse repetition

frequency (PRF) of 300 Hz, and the signal recorder was configured for unambiguous range of 300 km.

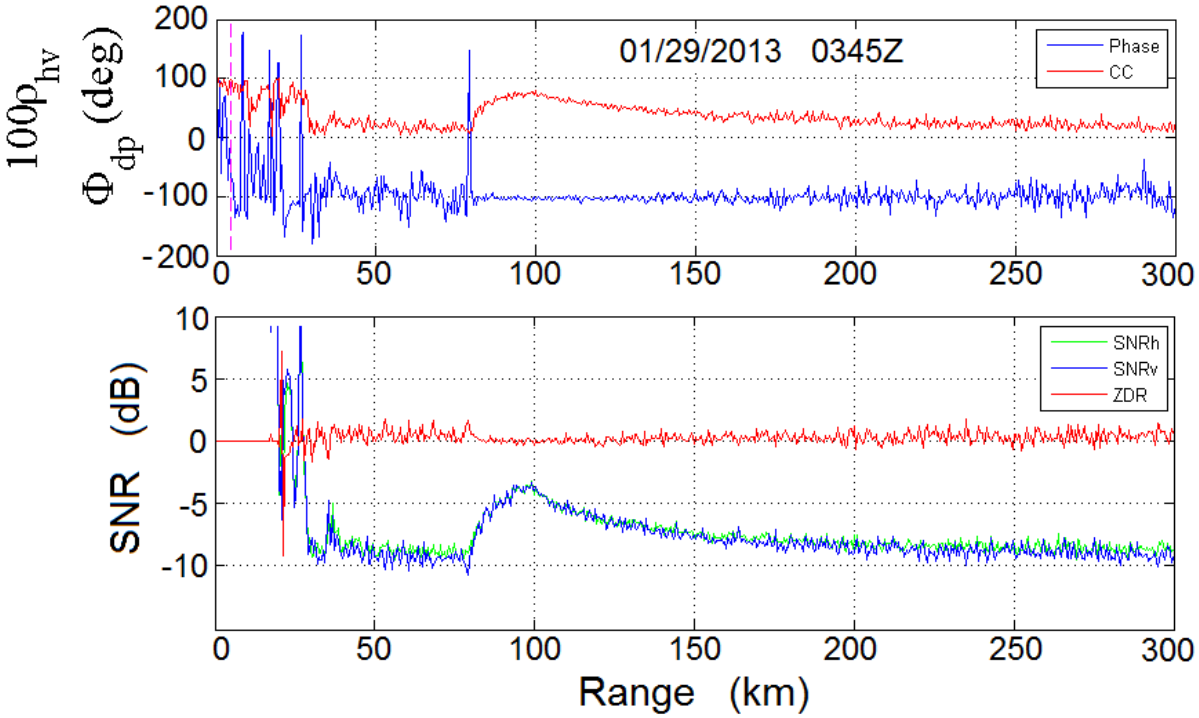

Fig. 4.13. (Upper panel): Range profiles of the differential phase Φ_{dp} (the blue line) and correlation coefficient $100\rho_{hv}$ (red line) for radar signals reflected from the Moon. Data collected 29 Jan. 2013 at 03:45 UTC. (Lower panel): Range profiles of SNR at horizontal (the green line) and vertical (blue line) polarizations. The Z_{DR} range profile is shown with the red line. The Moon was in 96% of visibility, i.e., almost the full Moon.

The distance to the Moon varies from 3.633×10^5 km (Perigee) to 4.055×10^5 km (Apogee) which is much longer than unambiguous radar range of 300 km so that the returned signal from the Moon can appear anywhere in the radar range profile. In Fig. 4.13 the Moon signal is at distances between 80 km and 200 km. The gradual decrease of the signal beyond 150 km is due to geometry of reflection from the rough Moon sphere (the equatorial radius of the Moon is 1738.1 km). The maximal returned signal is at distances about 100 km where $SNR_{h,v}$ are about 6 dB. The noise level was estimated with the antenna pointed away from the Moon. Z_{DR} in areas with maximal SNR is close to 0 dB. At these ranges, Φ_{dp} exhibits less fluctuations compared to other distances and its value of -101^o (in interval from -180^o to 180^o) is close to the system differential phase. Values of ρ_{hv} are ~ 0.7 and are significantly higher than at other distances. These properties can be used to identify return signals from the Moon.

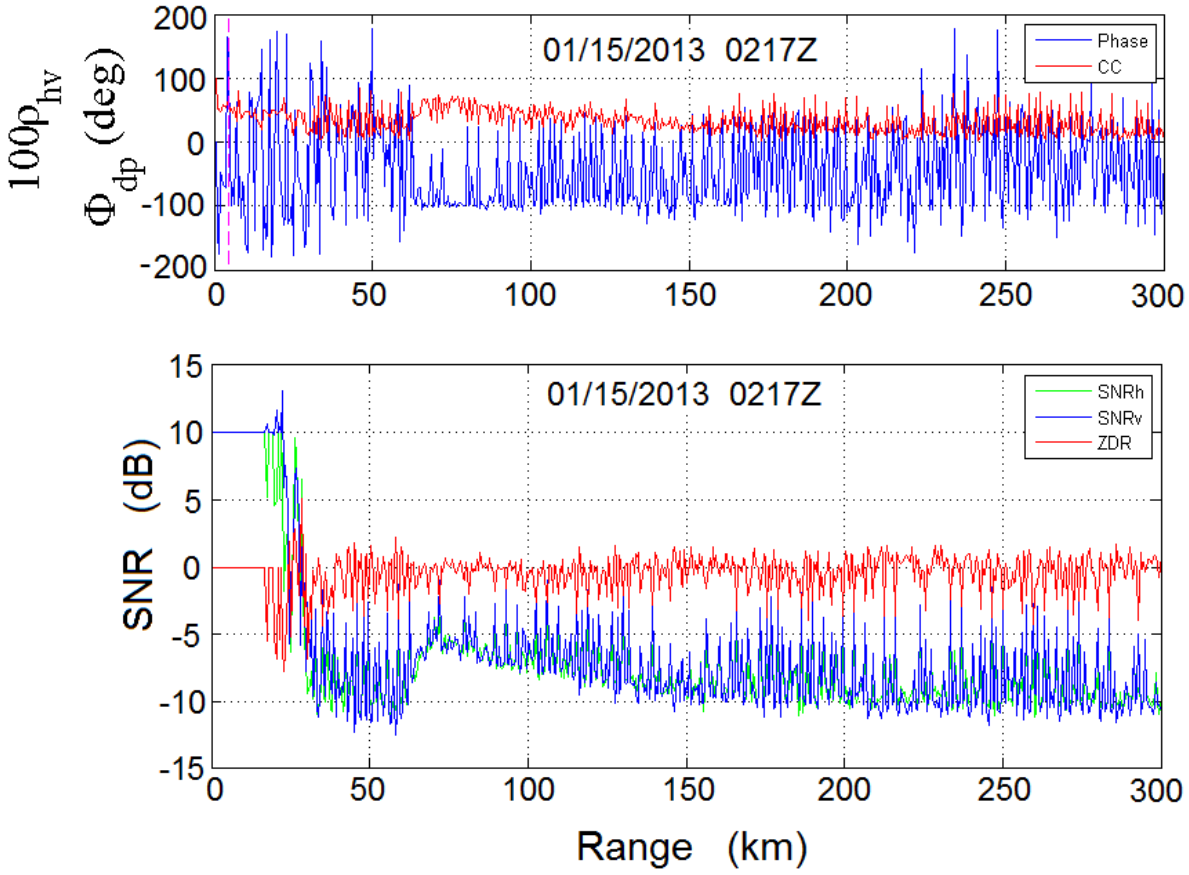

Fig. 4.14. Same as in Fig. 4.5 but for 15 Jan. 2013 at 02:17 UTC.

Fig. 4.14 exhibits some issues with the Moon observations. One of the main difficulties is interference signals which make the Moon signal "noisy". Since the Moon signal is weak, any interference signal worsens its detection. It is not clear how to overcome this problem in sites with many signal sources.

Another problem is the requirement of long observations of the Moon return signal. To obtain good estimates of Z_{DR} from the Moon, it is necessary to track the Moon with radar antenna. The time for signal to reach the Moon and get back is from 2.4 to 2.6 seconds. This requires tracking the Moon's center. The "boxcar" observations (like in case of the suncheck measurements) cannot be applied for the Moon.

The optimal pulse repetition frequency, longevity of the radar pulse (short or long), and various parameters that should be used in the Moon's observations need to be determined yet. Observations of the Moon are attractive because both transmit and receive radar circuits can be calibrated.

5. Summary and future work

Analysis presented in section 2 has not revealed a single major flaw in the Z_{DR} calibration procedure implemented by the contractor on the WSR-88D radars. That is there is no smoking gun, a step that we can blame for major calibration errors that are seen on some radars. Nonetheless, several issues have been identified and evaluated via tests on the KOUN and KTLX radars. These caused errors within the specified tolerance of 0.1 dB, but because the sample of two radars is very small there is no guarantee that similar performance is on the rest of the network. Overall the most troublesome is the complexity of the procedure. There are too many steps each of which introduces a small error. Here the whole is much worse than the sum of its parts (steps). Then there is the human factor. The probability of a human mistake is much higher if the procedure is complicated, consists of a large number of steps, and takes long time to complete. On few occasion it has been verified that large errors in Z_{DR} calibration were due to misunderstanding of the calibration process.

Obviously more needs to be done to resolve the calibration issue, and in the following we list some recommendations (in italics). There are grouped into short term (within one year), midterm (more than a year) and long term.

Short term recommendations

1. Reliance on manufacturer's specification (measurements) of coupling coefficients on the waveguides. There is not guarantee that all of these are correct. However each value should be good to about 0.02 dB.

It is desirable to completely eliminate any absolute value other than absolute differences in a sound differential measurement procedure.

2. Measurements of the receiver bias (RCB) and sun bias (SMB) are made with the transmitter off. Therefore the circulators are cooler and not in a state that they are when Z_{DR} measurements are made.

Ideally the measurements should be made with the transmitter on (section 3.1).

3. Manual operations (manipulations) in measurements of the transmitter bias (TXB), sections 3.2, 3.5.

An electronic switch should be considered.

4. The transfer characteristics of the two receivers. These can have a dependence on the SNR and if the variation across the fleet is small, similar to the KOUN and KTLX (section 3.4), then there should be no significant effect on the Z_{DR} bias. But if the variation is significant it could throw the sun scan measurements off (see next point).

5. Sun scan measurement. The SNR of the sun signal is typically between 10 and 15 dB, but could be lower. The Z_{DR} of the sum is extrapolated to high SNRs and if the nonlinearity at low SNRs is much worse than what we measured on KOUN and KTLX (Fig. 3.5) there will be a significant bias emanating from the wrong extrapolation.

Receiver non linearity and sun measurements should be checked on the radars that have notoriously poor Z_{DR} *calibration.*

6. Difference between wideband and narrow band measurements (section 3.6). Our measurements indicate that this was not a significant bias factor on KTLX but is about 0.1 dB for KOUN. Measurements on other WSR-88Ds are needed to evaluate the impact of this difference.

7. External sources for Z_{DR} calibration. Bragg scatter observations can be used to calibrate Z_{DR} and to control the calibration (sections 4.1 – 4.3). ROC has been doing just that, data filter to select Bragg echoes from other types of reflections using existing VCPs #31 and #12.

Design a distinct VCP *to observe Bragg scatter* (section 4.3).

8. Feasibility of using the returns from the Moon for relative Z and Z_{DR} calibration (section 4.4).

Explore this possibility.

9. Baron Services has a proprietary procedure that according to Mr. M. Balaji looks very promising.

If this procedure is revealed evaluate its potential.

Long-term recommendation

It was known to us and proven on the network and herein that "engineering calibration" might not be feasible on a large network as WSR-88D. By "engineering" we mean the procedure that requires absolute measurements as is currently done. We suggest readers look at the report "Calibrating the differential reflectivity on the WSR-88D" PART II (Zrnic et al. 2007, on the NSSL publication WEB site). There, the "differential" calibration is argued for and rational to ignore all but the receiver path is given. The report assumes a fixed power splitter and suggests 1) measurement of the split power at the well calibrated couplers as is currently done. Subsequently at TIM meetings we recommended that each splitter be measured in the factory and do away with measurement above the rotary joint.

In the long run the variable power divider in the transmission path should be replaced with a fixed power splitter. This would eliminate one variable in the measurement, the repositioning of the dielectric within the waveguide that supposedly assures precise division of the power into two equal parts. This repositioning occurs every eight hours or every time the transmitter is turned on. With a fixed divider the only variables in the transmission path is the difference in the attenuation by the two circulators. Even though the difference is small we recommend monitoring the relative difference of transmitted power as is done on the current WSR-88D. We recommend retaining automatic updated of the receiver calibration procedure at

the end of volume scans. To close the loop we suggest a manual injection into the RDA of the absolute correction obtained from either the Bragg scatter of drizzle. Here are the steps:

a) *Monitor the relative difference in gains of the transmitter paths* $T_h - T_v$ (dB) *above the circulators. Use the current procedure, to switch between the H and V couplers and use one receiver say H to measure the difference. Repeat back and forth the measurement to insure it is stable. This should be performed at 8 hour intervals. Keep track of the change in the relative difference at 8 hour intervals. This change is the correction that must be accounted for in the bias computation.*

b) *Monitor the relative difference in gains of the receiver chain at the end of each volume scan and compensate for the change exactly as currently implemented.*

c) *If the relative difference* a) *and the relative difference* b) *are kept constant then the true offset of* Z_{DR} *calibration would need to be found once and that could be done on targets of opportunity*

Midterm recommendation

This recommendation is equivalent to the long term one but could be implemented much sooner. In the nut shell, the variable power divider is not removed. Rather, the penetrating dielectric slab is put in a fixed position so that the power difference $T_h - T_v$ does not change. Technical evaluation of how to accomplish time invariant division remains to be determined.

Acknowledgments. The authors thank Dr. Jeffrey Cunningham, Mr. Walter Zittel, Mr. Richard Ice, Mr. Adam Heck, and Mr. Joe Crisman from the Radar Operations Center and Mr. Robert Macemon from the Baron Ltd for the valuable discussions and support that helped us to make the radar measurements and interpret the results.